
Politecnico di Torino

Politecnico di Torino

Department of Applied Science and Technology

# Dysprosium-doped carbon dots for magnetic resonance imaging and theranostic applications

Master's Degree in Biomedical Engineering

SUPERVISORS:

Prof. Alberto Tagliaferro

Dr. Mattia Bartoli

CANDIDATE:

Angelica Zucco

October 2022

# CONTENTS

# ABSTRACT

Magnetic resonance imaging is a powerful diagnostic tool that allows a precise investigation of the human body, anatomic structures, physiological functions, molecular composition of tissues, providing clear and three-dimensional images. The addition of a contrast agent has become a crucial step for enhancing image contrast. By speeding up the rates at which water protons relax in the tissues where the agent accumulates, magnetic resonance imaging contrast agents selective highlight structures or tissues in the body that could not be investigated otherwise. Contrast agents have received a lot of attention in terms of research and development pursuing the preparation of an imaging probe with adequate biocompatibility, good colloidal stability, improved relaxometric properties, and advanced functions. After the advent of nanotechnologies, the use of magnetic nanostructured agents has been the main focus of magnetic resonance imaging contrast agents' development up to this point. Nanoscale materials have shown outstanding physical and chemical properties due to the improvement of surface-to-volume ratio and the abundance of functionalization sites. Carbon quantum dots, also known as C-dots, are a novel type of nanomaterial that has been widely studied during the last few years. Due to their high fluorescence characteristics, strong biocompatibility, dimension, and low toxicity, carbon dots have been investigated as biosensors, gene transmitters, drug carriers, and bioimaging probes. Plus, their optical properties make them potentially suitable for environmental and biological sensing and imaging too.

The purpose of this work is the synthesis and characterization of dysprosium-doped carbon dots that could be suitable for magnetic resonance imaging contrast agent application. The evolution and recent development of imaging techniques have brought magnetic resonance imaging procedures to a higher level to adapt to the necessity of conducting imaging exams in shorter times and with higher resolution. The dysprosium cation ($Dy^{3+}$), having a high magnetic moment and short relaxation time, has been considered the best choice for contrast agents in high magnetic field magnetic resonance imaging. A bottom-up approach was adopted, and every set of carbon dots was produced using a one-step microwave-mediated synthesis method. Two main classes of carbon dots were synthesized: carbon dots from citric acid and dysprosium chloride hexahydrate and carbon nitride dots, in which urea was added as a nitrogen source. Then, it was applied a step of purification that included centrifugation, filtration, and dialysis. Characterization techniques such as UV–Vis and Fluorescence spectroscopy, Fourier-transform Infrared spectroscopy, Atomic Force Microscopy, Transmission Electron Microscopy, Zeta Potential analysis, Mass spectrometry, and Thermogravimetric analysis. Carbon quantum dots have shown a passive uptake in tumors and retention effect too and their dysprosium-conjugated derivatives could be used as theranostic tools. This new approach opens the way to both personalized medicine and imaging-guided therapy. In this context, the previously prepared carbon nitride dots were conjugated to doxorubicin, a chemotherapeutic drug largely used for treating, among others, blood, bladder, breast, lung and nerve cancers. For the conjugation process, EDC/NHS coupling was employed. The last step of the work included the analysis of the ground-state properties of carbon dots through Electron Paramagnetic Resonance and cellular imaging. First, viability tests were conducted on human healthy and cancer cell lines to assess the toxicity of both carbon dots and carbon nitride dots. Dysprosium is known to be potentially irritating, but the viability tests showed low toxicity levels. These results were further discussed to evaluate the next challenges and future perspectives of both selective bioimaging and theranostic applications.

# CHAPTER 1
# INTRODUCTION

## 1.1 MAGNETIC RESONANCE IMAGING AND CONTRAST AGENTS: PROPERTIES

### 1.1.1 Magnetic resonance imaging

The invention of magnetic resonance imaging (MRI) has been one of the major medical breakthroughs of the 20th century, making it possible to produce 3D images of the human body with outstanding soft tissue contrast and spatial resolution [1].

Originally developed as a spectrometric method used by biochemists, it was then applied in the diagnostic field, mainly in neurology; later its application was extended to all anatomical sites and different pathologies. This imaging technique allows a deep investigation of the human body, with a particular focus on tissue composition and body structures [2].

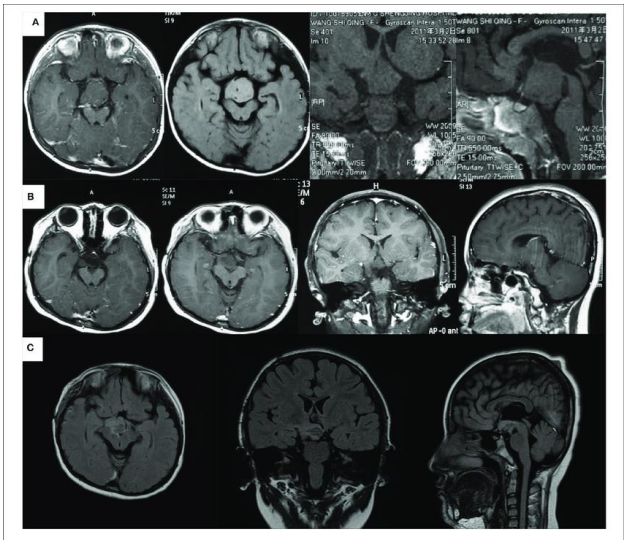


Fig. 1.1: Magnetic resonance images of the brain [3].

### 1.1.2 Physics of MRI

During an MRI analysis, the patient is exposed to a very strong magnetic field (as much as 10,000 to 15,000 times higher than the Earth's magnetic field), so that the protons gain energy and orient themselves according to the direction of the external magnetic field [1]. When the latter is turned off, the spins return to their natural orientation, releasing the accumulated energy and emitting a signal. Complex systems make it possible to capture that signal and extrapolate MR images from it [2,4].

To discover the physics behind a magnetic resonance procedure, it is fundamental to understand magnetism and how its definition in the field of classical physics can be applied to atoms too. The first

studies of magnetism have been conducted by four main scientists: Oersted, Ampère, Faraday and Maxwell [4,5]. As a result of their work, it was stated that a magnetic field can be generated both by a magnetic rod and a solenoid, i.e., a coil traversed by an electric current.

Nuclear magnetism can originate from all nuclei having an odd number of protons and/or neutrons. Hydrogen nucleus is at the basis of the magnetic resonance method [4,6]. Its proton rotates around its own axis and forms a magnetic dipole that is perturbed by the presence of an external magnetic field [4]. In quantum terminology, such motion is called spin.

To start a spin motion, a precise amount of energy is needed. The magnetic quantum number "m" defines the number of energy levels: for each m, there are 2m+1 energy levels. For hydrogen, m is equal to 1/2, meaning a total number of two energy levels. Therefore, hydrogen can occupy only two states when an external magnetic field, $B_0$, is applied: the lowest energy level when aligned with $B_0$ and the highest when aligned against it. Without the magnetic field, the two levels are degenerate. In quantum mechanics, two or more different states of the same quantum mechanical system are degenerate if they have the same energy value. This concept can be explained by the so called "Zeeman effect", which proves the remotion of degeneracy by the application of an external magnetic field [7].

More than 70% of the human body is made of water. Each water molecule has two hydrogen protons. MRI exploits this abundance of hydrogen protons: the application of the external magnetic field $B_0$, produces a net magnetization, M, of the hydrogen protons that is aligned with the direction of $B_0$. Then, through a radiofrequency pulse ($B_1$) this magnetization is perturbed. When the pulse ends, the magnetization comes back to its initial orientation. In this process, the two momentum components return to their original values: the longitudinal component returns to its maximum value, while the transversal component returns to zero. This process is called relaxation. The measure of the time (T1, T2) that the two components take to assume their original value is used to extrapolate the MR image. T1 is the time associated with the longitudinal component and T2 is associated with the transverse component. To keep $B_0$ uniform throughout the whole process, magnetic field gradients are applied [5,6].

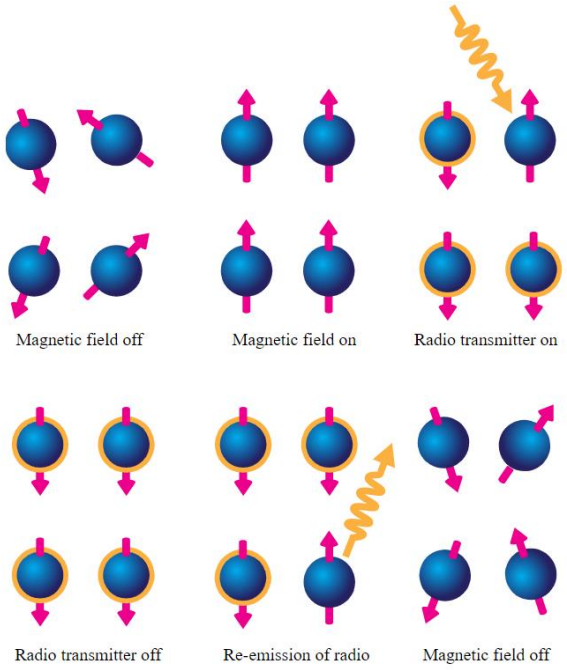


Fig. 1.2: Physics of MRI [7].

### 1.1.3 Instrumentation and process

MRI is a highly safe tool that is harmless to the human body [9]. The patient is not exposed to ionizing radiation, for this reason the tests can be repeated several times, even a short time apart.

The main components included in an MRI system are a computer system, a magnet, a radiofrequency system, and a data acquisition system. More in deeper, the newest MRI employs cutting-edge technology for radiofrequency excitation and detection as well as for producing significant magnetic field gradients. The gradient is a variation of the magnetic field over space. The gradient system produces variations that are overlaid on the primary magnetic field. The gradient system consists of gradient coils, typically one for each of the three axes (x, y, and z), which vary the magnetic field in a specific direction. For instance, if a gradient is applied parallel to $B_0$, the magnetic field will either be greater toward the subject's head and weaker toward the subject's feet, or vice versa [10].

The image is produced through a set of mathematical operations carried out by effective informatics systems [4,5]. In MRI, a coiled wire surrounding the instrument generates the magnetic field, which is measured in Tesla units. Super cooling fluids, such as liquid helium and liquid nitrogen, help to lower the temperature, reaching about -263°C. Most clinically used MRI systems apply magnetic fields between 1.5T and 3T.

The traditional MRI consists of a large, deep, hollow cylinder open at both ends, in which the patient can lie on a special sliding couch. In standard versions of MRI machines, the diameter of the central opening is 60 centimeters; in more advanced versions, however, it reaches up to 70 centimeters. One of the problems connected to the diameter concerns all the patients who suffer from claustrophobia. Open MRI is an alternative to classic MRI, in which, instead of cylindrical equipment, a C-shaped instrument is used, allowing more room for movement. Generally, MRI exams can last from fifteen to sixty minutes [9].


Fig. 1.3: MRI instrumentation [11].

### 1.1.4 Common uses of the procedure

MRI is a diagnostic tool that helps to extrapolate a large amount of information in different conditions and procedures. MRI provides clear and detailed three-dimensional images of soft tissues (nerves, muscles, ligaments, fat, blood vessels, etc.) and hard tissues (bone and cartilage). This makes it a relevant test in numerous fields of medicine: traumatology, oncology, orthopedics, gastroenterology, cardiology [5,9]. More in detail MRI allows the study of:

- brain and spinal cord abnormalities;
- breast, prostate, and liver abnormalities;
- joint injuries;
- cardiac structure and function;
- areas of activation within the brain (functional MRI);
- blood flow through vessels and arteries (angiography);
- chemical composition of tissues (spectroscopy).

Moreover, MRI can be used to guide some interventional procedures in real-time.

The clinical test is particularly good for studying soft tissues, and often it is preferred to a Computed Tomography (CT) scan because it does not employ harmful ionizing radiation. The brain, spinal cord, and nerves, as well as muscles, ligaments, and tendons, are much more apparent through MRI than on X-ray and CT scans, so this exam is often requested for knee and shoulder injuries too. In the brain, MRI can help to distinguish between white and grey matter and diagnose aneurysms and tumors. When physicians need to repeat examinations and screen frequently the patient, MRI is the imaging method of choice; however, it is significantly more expensive than X-ray and CT scan techniques [5,9,10].

### 1.1.5 Signal intensity and contrast agents

In MRI images, the signal intensity (brightness) of tissues is determined by:

- The radiofrequency pulses and gradients used to obtain the image
- The intrinsic T1 and T2 characteristics of different tissues
- The density of protons of different tissues

Often, it is necessary to use a contrast agent, especially when the physician needs to highlight vascular structures, inflammation, and tumors. The most used agents are gadolinium derivatives, which have magnetic properties that affect proton relaxation times. Contrast agents are injected intravenously just before the diagnostic test [9].

### 1.1.6 Advantages and risks

Essentially, the risks of MRI are mainly related to two aspects: magnetic field and contrast agent. The main risks include [5,6,9]:

1) People with implants, such as iron-pacemakers, vagus nerve stimulators, implantable cardioverter defibrillators, loop recorders, insulin pumps, cochlear implants, deep brain stimulators, and

endoscopy capsules cannot enter an MRI machine because the field generated could impair the device functioning;

2) Machine's noise could be hurtful for the hearing;

3) Gadolinium-based contrast agents cannot be used in patients affected with severe renal failure (this aspect will be further discussed);

4) Although no effects on the fetus have been demonstrated, it is recommended to avoid MRI scans as a precaution, especially in the first trimester of pregnancy;

5) People with even mild claustrophobia may have difficulty tolerating long scan times inside the machine. In severe cases, sedation or, if possible, the use of an open machine may be used.

# 1.2 READY TO BE USED: AVAILABLE CONTRAST AGENTS

## 1.2.1 Contrast-enhanced MRI

Adding contrast agents is a crucial step in enhancing MRI contrast. By speeding up the rates at which water protons relax in the tissues where the agent accumulates, MRI contrast agents improve the contrast between healthy and diseased tissues on an image and reveal the condition of organ function or blood flow after treatment [9,12].

Contrast agents are useful to highlight body structures and tissues that could not be seen without the injection of the contrast media. Contrast agents are essential to distinguish the selected area of interest from the surrounding tissues [12,13].

In 1988, the first MR contrast agent was made available for imaging blood-brain barrier disorders. Recently, contrast-enhanced MRI has grown in significance in the field of diagnostic medicine. Worldwide, tens of millions of contrast-enhanced exams are requested each year. In addition to many other uses, contrast-enhanced MRI is now frequently utilized to image lesions in the breast, abdomen, and central nervous system as well as for angiographic, cardiac, and articular imaging [13,14].

The majority of available MR contrast agents are gadolinium complexes. Some of them were initially synthesized and used for imaging of the central nervous system [14]. The original and currently gadolinium-based contrast agent, Gd-DTPA (gadolinium-diethylenetriamine pentaacetic acid) or Magnevist™, was approved about thirty years ago. There are currently eleven different contrast agents that can be used intravenously, according to the US Food and Drug Administration (FDA) [8,12,13].

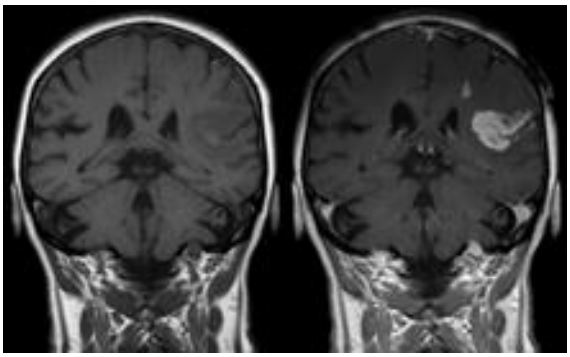

Fig. 1.3: MR image before and after Gadolinium injection [15].

## 1.2.2 Classification

MRI contrast agents can be classified following different parameters. It is possible to categorize them according to their biodistribution and applications, their magnetic properties (paramagnetic, superparamagnetic), and their mechanism of action (T1, T2).

### 1.2.2.1 BIODISTRIBUTION AND APPLICATIONS

MR contrast agents can be administered either intravenously, orally, or by inhalation [12,13,14]. The distribution of the agent is exploited by the contrast enhancement seen after injection, and extracellular agents are often the best options for spotting diseased tissue. For instance, hypervascularity, impaired endothelium, and/or an underdeveloped lymphatic drainage system are typical characteristics of tumors that cause them to momentarily retain higher concentrations of the contrast agent than healthy tissue and for longer periods of time [14].

More in detail the enhanced permeability and retention (EPR) effect is a particular phenomenon that takes place in solid tumors and is associated with their unique anatomical and pathophysiological features, such as inefficient lymphatic system, and abnormal vasculature, including abundant vascular mediators like bradykinin, nitric oxide, carbon monoxide, and vascular endothelial growth factor [16]. For this reason, a lot of tumor tissues exhibit significant extravasation of plasma and nanomedicines. However, EPR effect may not be applicable to all solid tumors [14,16,17].

Minutes after injection, the contrast agent clearly enhances the contrast of the tumor. By getting scans while contrast agents are first passing through the arteries or by monitoring the accumulation of the contrast agent in the tumor, significant information can be discovered [12,13,14].

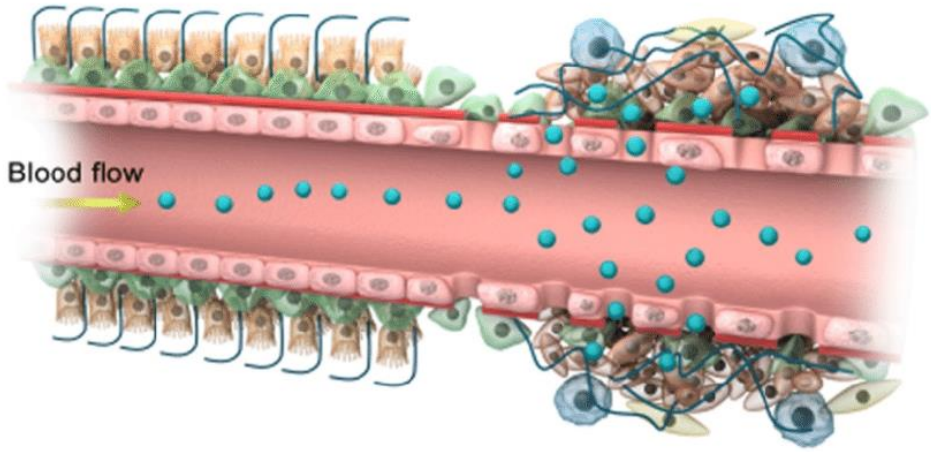


Fig. 1.4 : Nanoparticles penetrate the tumour via EPR effect [18].

**Oral agents** are indicated for gastrointestinal tract imaging. Gadolinium and manganese-based agents, SPIOs, and barium sulphate suspensions have been investigated as potential agents. However, this type of contrast agents is not widely used.

**Ventilation agents** are contrast agents that are suitable for lung imaging. Basically, they consist of gadolinium(III)-based aerosols and oxygen gas.

**Intravenous MRI contrast agents** can be divided into three types [19,20]:

- EXTRACELLULAR FLUID AGENTS (ECF)
  These agents are dispersed between the cellular and intravascular regions. ECF agents are low molecular weight chelates that enter the extravascular and extracellular space after being injected intravenously, travel to the heart, and then exit through the systemic arteries. Through the renal route, they leave the body quickly. The majority of contrast agents sold in the United States, or >98% of all contrast agents, are ECF agents. They are typically used to detect changed tissue endothelium and vascular abnormalities (i.e. disrupted blood brain barrier) [14,19].

- BLOOD POOL AGENTS
  After the injection, these agents remain in the intravascular area and offer excellent contrast when used to image the arteries and veins. Many blood pool agents were being developed in the 1990s [19,20]. Three primary approaches were used, and all of them produced substances that underwent human clinical trials: (1) Substances with a low molecular weight that, upon intravenous injection, bind noncovalently to human serum albumin (commercial products: Angiomark, Vasovist, and Ablavar). (2) Gadolinium-based compounds that exit the endothelial barrier but are still small enough to be filtered by the kidney. (3) Small iron oxide nanoparticles with high T1 relaxivity that remain in the blood circulation for a long-time and then accumulate in the liver and spleen where the iron can be incorporated [14,19].

- TARGET/ORGAN SPECIFIC AGENTS
  These agents can target specific organs or tissues and are eliminated through the kidneys. This can be done by functionalizing the agent with a specific ligand to target a pre-determined condition (i.e. tumour tissue).

#### 1.2.2.2 MAGNETIC PROPERTIES: MECHANISM OF ACTION

Currently used MRI contrast agents can be divided into superparamagnetic agents and paramagnetic agents based on their magnetic properties [20].

- PARAMAGNETIC
  The most used MRI contrast agents by far are paramagnetic contrast agents [23]. Enhancing the MR contrast in the areas where they are distributed, they are also known as positive or negative contrast agents. Commonly, paramagnetic contrast agents are metal ions with unpaired electrons, such as the transition and lanthanide metal ions. These include gadolinium ($Gd^{3+}$), manganese ($Mn^{2+}$ and $Mn^{3+}$), iron ($Fe^{2+}$ and $Fe^{3+}$), lanthanide ($La^{3+}$), and dysprosium ($Dy^{3+}$), and many others. Gadolinium-based contrast agents are the most used, especially because gadolinium has seven unpaired electrons, symmetric electronic states, strong relaxivity, and a total coordination number of nine. However, due to their undesirable biodistribution and relatively significant toxicities, paramagnetic metals cannot be utilized as contrast agents in the ionic form. Because of this, powerful chelates made of ligands complexed with paramagnetic metal ions remain stable in the body minimizing the risk of side effects [12, 14, 19,21].

- SUPERPARAMAGNETIC
  Superparamagnetic contrast agents consist of colloidal substances with particle diameters between 5 and 200 nm. These particles contain tiny crystallites (1–10 nm) that have hundreds of randomly aligned magnetic ions, mainly iron. In the superparamagnetic particles, the crystallites align with the magnetic field in the presence of an external magnetic field, creating a superspin that makes the substance magnetic [14, 21]. The particle has a substantially bigger total spin than the sum of its constituent metal ion spins, which can lead to an extremely high relaxivity [21]. The substance is no longer magnetic in the absence of the applied field. The crystallites are made of an iron oxide core that can be coated with various materials, such as dextran, citrate, carboxydextran, chitosan, starch, heparin, albumin, polystyrene or other non-immunogenic polymers [14, 21]. The early superparamagnetic contrast agents mostly affected T2 and had extremely high r2/r1 ratios. These materials produce darkened MR images so they are sometimes known as T2-agents or negative contrast agents. However, there are numerous instances of superparamagnetic iron oxide particles that can function as T1 or T2 contrast agents and have a significant r1. According to the size of the particulate, superparamagnetic iron oxides can be divided into three groups: (1) ultrasmall superparamagnetic iron oxide (USPIO) particles, (2) small superparamagnetic iron oxide (SPIO) with a diameter of less than 50 nm, and (3) micron-sized iron oxide (MPIO), which have a diameter greater than or equal to one micron [12, 14, 19, 20, 21].

#### 1.2.2.3 RELAXATION MECHANISM (T1, T1)

There are several contrast mechanisms that exploit the tissue's differences. For instance, the relaxation times T1, T2, T1ρ (T1 in the rotating frame) can be very different in adjacent tissues and images can be acquired using pulse sequences that are weighted to provide more (or less) signal intensity for a short relaxation time. Contrast can also be generated from physicochemical properties of water such as diffusion and flow. The majority of contrast agents serve to shorten the relaxation times of water, while CEST agents exploit a saturation transfer mechanism [14, 21].

For the purpose of this project, it is important to mention that available MRI contrast agents can be categorized mainly into two broad groups: T1-agents and T2-agents. T1-agents generally increase the longitudinal (or spin-lattice) relaxation rates (1/T1) of water protons in tissue more than the transverse (or spin-spin) relaxation rates (1/T2). With most conventional pulse sequences, this dominant T1-lowering effect increases the signal intensity predominant on T1 weighted images; thus, these are positive contrast agents. On the other hand, T2-agents largely increase the 1/T2 of tissue leading to a decrease in signal intensity, predominant on T2 weighted images, thus these represent negative contrast agents. The relaxivity of a contrast material determines its efficiency in reducing the T1 and T2 relaxation times [14, 25].

Other types of contrast agents can also be used but they are less common. This is the case of non-proton agents, such as certain perfluorocarbons. They do not affect relaxation rates but produce low signal intensity thanks to the absence of hydrogen [12, 14, 19, 20].

### 1.2.3 Standard of care

Chemistry and biochemistry researchers have largely contributed to the development of contrast agents in the last few years[27]. There are numerous requirements for the design of a contrast agent, such as low toxicity, adequate relaxivity ratios, good colloidal and simple administration to the patient. New types of probes that produce good results are largely needed right now as reported in Table 1.

| CONTRAST AGENT | GENERIC NAME | CHEMICAL COMPOUND | CONTRAST MECHANISM | APPLICATION |
|---|---|---|---|---|
| **MAGNEVIST** | Gadopentetate Dumeglumine | Gd-DPTA | T1 | Neuro/whole body |
| **GADAVIST** | Gadobutrol | Gd-DO3A-butriol | T1 | Neuro/whole body |
| **DOTAREM/ANTIREM** | Gadoterate Meglumine | Gd-DOTA | T1 | Neuro/whole body |
| **PROHANCE** | Gadoteridol | Gd-HP-DO3A | T1 | Neuro/whole body |
| **MULTIHANCE** | Gadobenate Dimeglumine | Gd-BOPTA | T1 | Neuro/whole body |
| **OMNISCAN** | Gadodiamide | Gd-DTPA-BMA | T1 | Neuro/whole body |

| | | | | |
|---|---|---|---|---|
| **OPTIMARK** | Gadoversetamide | Gd-DPTA-BMEA | T1 | Neuro/whole body |
| **PRIMOVIST** | Gadoxetic acid | Gd-EOB-DTPA | T1 | Liver |
| **TESLASCAN** | Mangafodipir Trisodium | MnDPDP | T1 | Liver |
| **VASOVIST (EUROPE)** | Angiomark, MS-325 | Gd-DTPA derivative | T1 | Angiography |
| **ABDOSCAN** | Ferristene | SPIO | T2 | Gastrointestinal |
| **GASTROMARK/LUMIREM** | Ferumoxsil | SPIO | T2 | Gastrointestinal |
| **RESOVIST/CLIAVIST** | Ferrixan | SPIO | T2 | Liver |
| **FERIDEX/ENDOREM** | Ferumoxide | SPIO | T2 | Liver |
| **IMAGENT GI/PERFLUBRON** | Perfluorochemicals | Perfluorooctylbromide | Replacement of water | Gastrointestinal |

Table 1.1: Available MRI Contrast Agents [13].

MRI contrast agents are a quiet new field. In particular, Magnevist, the first approved MRI contrast agent, acquired FDA approval in 1988 for contrast-enhanced MRI of the central nervous system (CNS) [19, 21]. Its use was later expanded to the whole body, excluding the heart, in 1993. Other agents were then approved: ProHance (Gd-HP-DO3A) in 1992; Omniscan (Gd-DTPA-BMA) in 1993; and Optimark (Gadoversetamide) in 1999 [27]. In addition, five other contrast agents received the approval: MultiHance in 2004 (Gd-BOPTA), Eovist (Gadoxetate) and Ablavar (formerly Vasovist, MS-325) in 2008, Gadavist in 2011 and Dotarem in 2013; some of them were approved in Europe and later in other parts of the world [23]. Regarding the non-gadolinium-based contrast agents, only two have been approved for intravenous use: Feridex and Teslascan. Feridex consists of dextran-coated iron oxide nanoparticles while Teslascan is made of mangafodipir trisodium. However, neither of these two are commercially available anymore [19, 22, 23, 27].

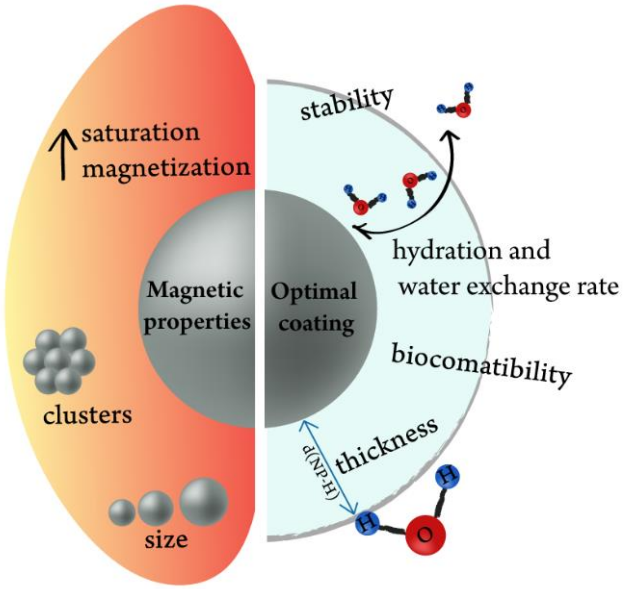


Fig. 1.5: MRI T2 contrast agents' requirements [22].

# 1.3 LIMITATIONS OF CURRENT MATERIALS

## 1.3.1 Requirements and limits

An MRI contrast agent must effectively decrease the T1 and/or T2 in tissues at low concentrations (mM to mM) with adequate tolerance. The key characteristics of paramagnetic MRI contrast agents are outlined in this paragraph, with an emphasis on GBCAs since they are the main class of agents that are currently clinically available on a global scale [12].

*High Relaxivity*: The "relaxivity", r1 and r2, of any agent is its basic capacity to reduce T1 and/or T2. At similar doses, a substance with a higher relaxivity will lower the T1 and/or T2 more than a substance with a lower relaxivity. This advantage allows for the possibility of lowering the dose or increasing the signal at equivalent concentrations, thus reducing toxicity and/or enhancing lesion identification or delineation [12,24,28,29].

*High Stability:* GBCAs are made up of transitional (heavy) metal Gd ions ($Gd^{3+}$) that have been securely bonded by chelating agents to produce a stable complex, which lessens the significant inherent toxicity of the free metal ion [28]. Small, water-soluble substances make up the agents. Stability here refers to the chelating agent's capacity to keep the Gd ion from being lost. Minimizing Gd dissociation from the chelating agent during the MRI contrast agent shelf-life and its dissociation in vivo are both critical to preserve an agent's low toxicity.

Specific biodistribution: It refers to the distribution of contrast materials to specific organs or tissues with a higher concentration than to other tissues, thereby reducing the necessary contrast material dose and/or raising the sensitivity of lesion detection. Agents that utilize the hepatobiliary, renal, or both renal and hepatobiliary modes of excretion are now available. Biologic target-specific contrast compounds are being investigated for application in imaging biochemical processes at the cellular and molecular levels [12, 19, 25, 28].

*Rapid Clearance:* After injection and subsequent imaging, MRI contrast agents should be quickly and significantly eliminated from the body. This is required to stop the slow deposition of dissociated free metal ions in certain tissues or organs, which causes chronic toxicity. With the exception of places where natural barriers (such the blood-brain barrier) prohibit it, these drugs spread quickly to extracellular areas. The quicker the clearance, the better in this case since no Gd chelate is completely resistant to Gd dissociation. Current medications come in doses of mmoles (25–300 mmol/kg of body weight, or multiple gram masses) [12,25].

*Low Toxicity*: Contrast agents should have low acute toxicity and not cause allergic or anaphylactoid reactions, alterations in normal blood values, or other immediate side effects. Specific patient populations with renal impairment, require special attention [12].

## 1.3.2 Safety concerns

Over the past three decades, a high number of contrast agents have been developed for use in clinical practice, and some of them have been removed from the market due to safety concerns. The chemical composition, presence of metal atoms, mode of administration, magnetic characteristics, biodistribution are some of the factors that can be used to categorize and study the agents. Analysing these factors, it is possible to extrapolate the therapeutic implications, mechanisms of action, safety, pharmacokinetics, and pharmacodynamics of these contrast agents [19, 21].

In the last few years, the creation of multifunctional, targeted, and responsive agents, as well as high sensitivity contrast agents for high magnetic fields and safe probes for patients with kidney diseases, show how much potential there is in the field of contrast agents for MRI.

Extracellular fluid contrast agents, and even blood pool contrast agents, have likely served their clinical purpose. This does not imply that the agents' poor sensitivity has been fixed. It is still difficult to find gadolinium-based contrast agents in vivo at local concentrations in the μM range. Therefore, the production of contrast agents with high relaxivity (>100 $mM^{-1}Gd^{-1}s^{-1}$) at high to ultra-high magnetic field (3-16.4T) strengths continues to be a research area of interest for chemists [19, 23].

Regarding toxicity issues, one of the main problems is related to GBCAs. In fact, they can be very dangerous and cause serious issues in people affected by chronic renal diseases such as nephrogenic systemic fibrosis. Iron oxide nanoparticles and molecular iron and manganese complexes are some of the options currently being considered but the optimal solution has not been found yet. Accumulation is another safety issue that must be considered. In particular, in gadolinium-based contrast agents, gadolinium ion ($Gd^{3+}$) is chelated to a ligand to increase the stability and avoid accumulation of the toxic ions. However, through the process of transmetallation that takes place in the body, endogenous cations ($Ca^{2+}$, $Zn^{2+}$, $Cu^{2+}$, $Fe^{3}$+) replace the $Gd^{3+}$, which detaches from the ligand and the risk of accumulation increases. Gadolinium ions can deposit in many tissues such as brain, liver, muscle, heart, lung, pancreas and bone and the degree of accumulation depends on its tissue [19, 23, 24].

These safety issues make it difficult to have a strict and solid regulatory status. In fact, the regulatory framework of contrast agents is not well-defined and needs more clarity. The FDA guidelines point out that all MRI centers have to provide Medication Guide to the patient the first time he/she receives a gadolinium-based contrast agent injection.

## 1.4 NANOSTRUCTURED CONTRAST AGENTS

MRI imaging probes with adequate biocompatibility, good colloidal stability, improved relaxometric properties, and advanced functions are in high demand given the state of MRI technology today. As a result, MRI contrast agents have received a lot of attention in terms of research and development. Different inorganic-based nanoprobes with inorganic magnetic nanoparticles (MNPs) and an organic functional coating have been developed recently to achieve the desired contrast augmentation effect [26, 27, 30]. The organic functional coating is essential for biomedical applications to increase colloidal stability and biocompatibility [26, 30]. The use of magnetic nanostructured agents has been the main focus of MRI CAs development research up to this point thanks to remarkable advancements in materials science [26, 30]. These studies are based on the observation that materials with nanoscale dimensions have special physical and chemical characteristics because of the improvement in surface to volume ratio and the abundance of opportunities to further functionalize them to tune them to the required specifications for the application. There are two ways to create the nanosized MRI CAs: either by enclosing the paramagnetic center within the nanoparticle or by conjugating the center to nanocarrier components [26, 27, 30, 32].

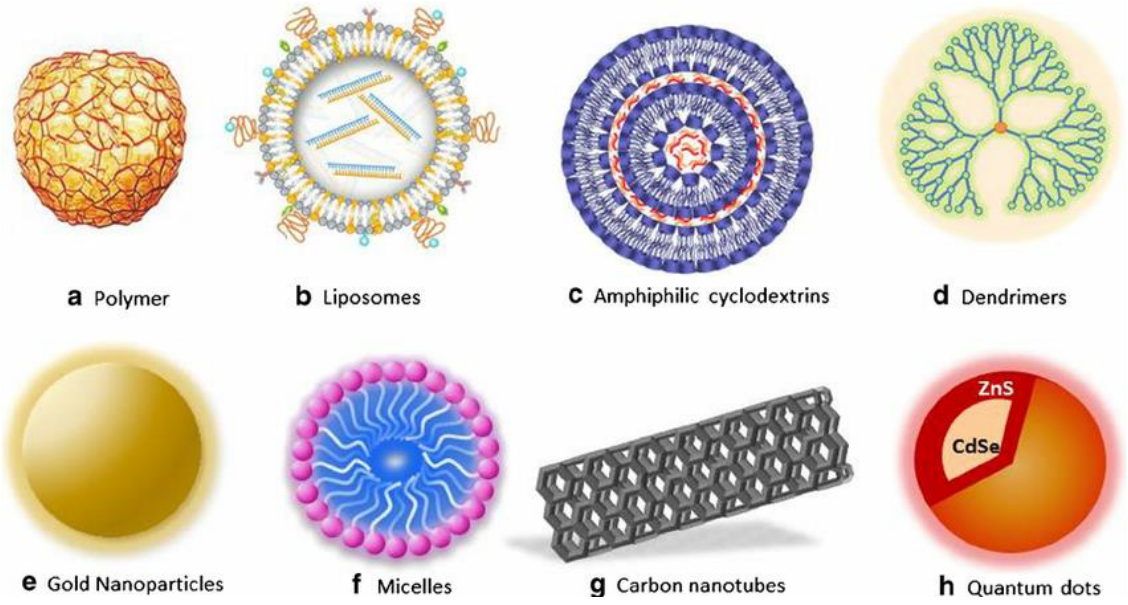


Fig. 1.6: Nanostructured agents [31].

## 1.4.2 Advantages of the nanoscale

Nanotechnology derives from the change of the characteristics of a material when split from bulk size into smaller sizes. Recently, nanomaterials have contributed to the development of many areas of manufacturing, and their great potential in medicine could bring substantial changes in the next few years. Scientists do believe that nanomaterials can be distinguished in part by their extremely small size, that should be less than 100 nm. However, it is not just a matter of size. The advantages and benefits of the nanotech world are also related to the changes that the physical, chemical and structural characteristics of materials undergo as they move from their natural forms to nanoscale forms. The overall result is that the material at the nanoscale turns out to be different from its natural dimensions. When talking about nanoparticles, the most relevant property is the ratio between the surface and the volume. Nanoparticles have a high ratio surface/volume, and it is the surface that influences the chemical and physical properties of the particles themselves, to the point of improving their structure and functionality [26, 30, 32].

## 1.4.3 Classification of nanostructured contrast agents

In the following part, the most used and known nanostructured contrast agents will be mentioned and briefly studied.

- MESOPORUS SILICA NANOPARTICLES: Mesoporous materials have lately undergone extensive research as biomaterials, such as carriers for regulated delivery of bio-active principles, due to their high specific surface, volume, and distinctive pore size. Mesoporous silica materials are adequate for drug loading and slow release of biomolecules. The inclusion of gadolinium in these particles helps the exchange of water hydrogen atoms with magnetic centre reducing the T1 and T2 relaxation times [33, 34].

- POLYMER BASED NANOCARRIERS: For the integration of gadolinium chelates as nanoscale CAs for MR imaging, a variety of polymer-based nanocarriers, including polymeric micelles, nano-hydrogels,

polymeric particles have been recently investigated. Polymeric particles are excellent candidates for image-guided therapy because of their superior advantages in increasing water solubility, reducing toxicity, increasing biodegradability, enhancing circulation half-lives and being simple to conjugate with various motifs [33].

- PLASMONIC NANOPARTICLES: Because of their adaptable synthesis process, physiochemical features, and outstanding biocompatibility, plasmonic nanoparticles have also drawn a lot of attention in biological research and applications. Plasmonic nanoparticles exhibit strong interaction with light through localized surface plasmon resonance (LSPR). This phenomenon occurs when electron oscillations in the conduction band of the plasmonic material resonate with the incident electromagnetic field [35]. Gold (Au) and silver (Ag)-based nanomaterials have been used in bio-imaging, cancer targeting, and cancer therapy because of their special localized surface plasmon resonance capabilities. Theranostic nanoparticles have been produced by conjugating drugs and small molecules (such as GBCA) for image-guided therapy [27,33, 24].

- IRON OXIDE NANOPARTICLES: Due to their numerous uses in magnetic hyperthermia for the treatment of certain tumors and as contrast agents for magnetic resonance imaging, magnetic iron oxide nanoparticles (MIONs) have a great potential in the biomedical field. There are numerous techniques available now for creating MIONs. The majority of MRI tests showed an effective contrast: these nanoparticles especially accumulated in the extravascular space of the organs. The recently discovered very small MIONs (ES-MIONs) smaller than 5 nm could be used as positive contrast agents, and MIONs larger than 10 nm can be employed as negative contrast agents [26, 33, 34].

- CARBON DOTs; The last class of nanostructured contrast agents consist of carbon dots. This topic will be further analysed in Chapter 1.6.

# 1.5 THERANOSTICS

Theranostics refers to the integration of a diagnostic method with a specific therapeutic intervention. This definition includes numerous diagnostic-therapeutic approaches (i.e. image-guided radiotherapy). However, it is usually restricted to those techniques in which the diagnostic method is developed simultaneously with the therapeutic intervention. Such methods have historically been developed in the field of nuclear medicine; but the latest innovations in the field of nanotechnology are also making it possible to create contrast agents with therapeutic characteristics [35,36].

Theranostic approach is centered on providing individualized patient care. The trend over the past several years has been toward customized care, which entails "custom-made" therapy that is based on each individual patient rather than being generalized for a group of patients. It is well recognized that a variety of factors that differ from person to person influence the development of tumors, neurological and cardiovascular diseases. Experts say that personalized therapy would help to reduce some of the risks connected to generalized therapy, such as failure, deaths, and high costs [37]. Furthermore, a patient's response to a drug is significantly influenced by their age, gender, nutrition, genetics and lifestyle [35, 36, 37].

Theranostic anticancer agents could be made from newly synthesized nanomaterials, and these materials also work well when imaging treatments like heat, radiation, or drug delivery are combined with therapy. The development of a biocompatible system that combines precise diagnostics with effective medicine delivery is still a major area of research. Theranostics' central tenet in 1940 was the use of radioiodine to detect and treat thyroid gland cancers.

Theranostics can make extensive use of liposomes, polymeric nanoparticles, metallic nanoparticles, and quantum and carbon dots. Various nanomaterials are easily functionalized with both medications to treat these illnesses as well as ligands to target certain organs, tissues, tumors, inflammations, and biologically harmful pathways. The synthesis, functionalization, and release of the medication can be done in a variety of ways. In general, scientists strive to prevent a drug's rapid release (burst release). As a matter of fact, numerous methods have been developed over the years to regulate the drug release over time in order to provide a consistent and steady course of treatment [36].

Recently, researchers have identified nanostructured MRI contrast agents as potential theranostic tools.

The process for the creation of contrast materials for MRI usually takes a lot of time. Beyond the various contrast agents which have been approved for use in humans, there are a significant number of new agents in clinical and research development [36]. To create paramagnetic and superparamagnetic nanoparticles with control over their composition, size, and form, a wide range of fabrication techniques are available. Furthermore, the ability to integrate additional imaging modes or drugs for treatment, and the use of specific vectors linked to the particle surface, make these agents yet more promising. More recently, high aspect ratio nanowires (NWs) and synthetic antiferromagnets (SAFs) have also been proposed as MRI contrast agents [36, 37]. The development and comprehension of different magnetic effects are of the uttermost importance in the pursuit of novel contrast agents in MRI. On the other hand, systematic in vivo studies are also needed to understand their mechanism of action and accumulation in different organs [36].

The final goal of theranostics is the design of a nanostructured system able to identify, penetrate and treat a tumor. Identifying and targeting a tumor can be realized using nanocarriers that selectively deliver the drug to the site of action. The choice of the target depends on the type of cells that need to be reached and targeted, but also on the type of drug that needs to be delivered. Different strategies have been applied in this context, such as the functionalization with aptamers, ligands, genes, and substrates for tumor markers.

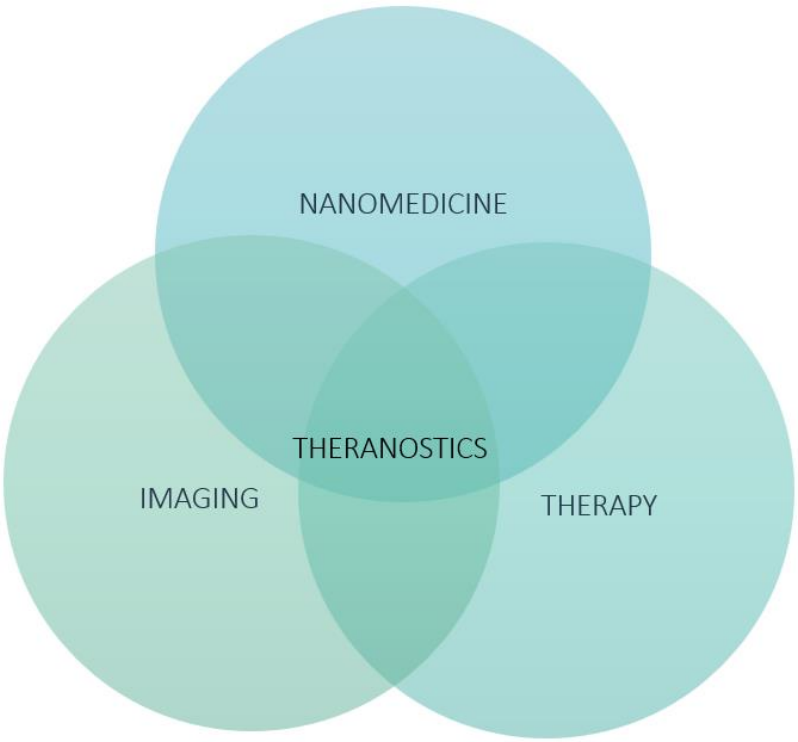


Fig. 1.7: Theranostic s as a combination of imaging, therapy, and nanotechnology [38].

# 1.6 CARBON NANODOTS: PROPERTIES AND MRI APPLICATIONS

Carbon dots (CDs), also known as C-dots, are a novel type of fluorescent material that has been widely studied in the last few years. Due to their high fluorescence characteristics, strong biocompatibility, dimension, and low toxicity, carbon dots have been investigated as biosensors, gene transmitters, drug carriers, and bioimaging probes. Plus, their optical properties make them potentially suitable for environmental and biological sensing and imaging too [39].

A wide variety of raw materials can be used to make CDs, and they are particularly appealing because of their strong chemical inertness and the numerous surface carboxylic groups that cause excellent water solubility and make it easier for them to be functionalized with organic, polymeric, inorganic, or biological species [40].

## 1.6.1 Structure and properties

CDs are defined as nanoparticles, mainly composed of carbon, with a size below 10 nm [40].

The centric carbon core structure of these particles is made up of sp2/sp3 carbon atoms. Due to the varying levels of carbonization the structure may exhibit graphite lattice or amorphous carbon form. Additionally, CDs' durability is improved by their covalent carbon skeleton structure, which is crucial for practical application. Compared with organic dyes and other conventional quantum dots, CDs not only have higher photoluminescence quantum yield and better light stability (resistance to light decomposition, photobleaching, and photoblinking), but also lower toxicity, lower costs and excellent biocompatibility [41].

CDs show a high number of surface groups, such as hydroxyl, carboxyl and many others. For this reason, they have optimal water solubility, being mainly hydrophilic, and they easily compose with other materials without phase separation. Furthermore, these groups allow the functionalization of the carbon dots with molecules, ligands, drugs [40, 41].

CDs are largely employed in many fields thanks to their outstanding properties. The most relevant characteristics include electrical conductivity, heteroatoms doping (such as nitrogen, phosphorus, sulfur etc.), optical properties (making them useful tools for biosensing and therapy development), phosphorescence, chemiluminescence and electrochemiluminescence, absorption and fluorescence properties that will be further discussed.

Regarding absorption, the short-wavelength area of the electromagnetic spectrum is where CDs' absorbance is produced because of the $\pi-\pi^*$ transition of unsaturated carbon- carbon bonds. CDs exhibit strong optical absorption in the UV band, between 260 and 320 nm. Usually, the absorbance range can vary according to the kind of CDs and their surface functional groups [39, 40].

Photoluminescence is one of the most relevant properties of Carbon Dots, making them very interesting for medical research, especially in the field of sensing and imaging. In Fig. 1.8, the process of photoluminescence is presented. Photoluminescence consists of the emission of light by a substance after the absorption of electromagnetic radiation. When a material absorbs a photon, an electron is excited and switches to a higher electronic state. Then, when the electron returns to a lower energy state, a photon is emitted. Photoluminescence includes both fluorescence and phosphorescence and it originates from an absorption/emission process between different electronic energy levels in the material. The amount and type of photoluminescence depend on the material and the wavelength used [40, 43].

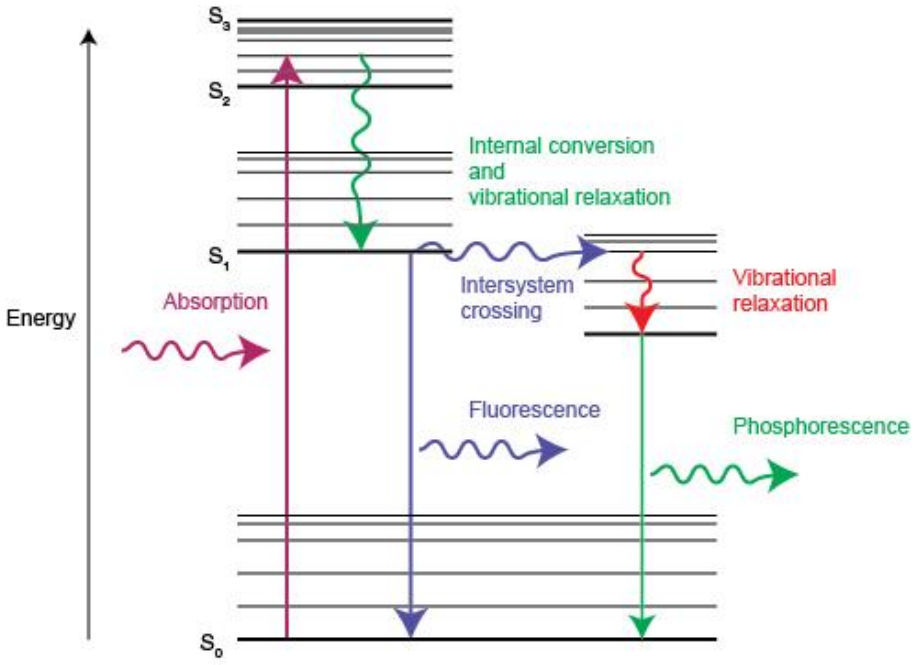


Fig. 1.8: Photoluminescence [42].

Concerning fluorescence properties, different CD fluorescence emissions can be produced by adjusting the excitation wavelength, which is possible by manipulating a number of physicochemical variables during the synthesis of CDs. For instance, pH, concentration, and temperature all have a significant impact on the fluorescence of CDs [43].

## 1.6.2 Synthesis methods

Due to the development of synthesis methods and the abundance of raw materials (graphite, small molecules, polymers, even natural materials, etc.), a large family of CDs formed up rapidly [41, 44].

The two main synthesis methods are “top down” and “bottom up”: these two techniques are used for a large variety of nanoparticles and they are not limited to the creation of C-dots. In general, top-down approach consists of transforming a bulk material into small nanosized particles, while bottom-up is a constructive technique and it is the exact opposite of top-down method [46]. There are multiple techniques that can be adopted for the preparation of carbon dots, such as the arc-discharge method, microwave pyrolysis, hydrothermal method, and electrochemical synthesis [47].

### 1.6.2.1 TOP-DOWN

In the "top-down" technique, bulky carbon compounds including carbohydrates, carbon fibers, activated carbon, etc. are cut or broken-down using chemical, electrochemical, or physical methods. The dissolution of the connection between the carbon atoms is essential to the overall formation mechanism. Strong oxidants like H2SO4 or HNO3 can oxidize and break down these large-sized carbon compounds into nanosized CDs [45].

1.6.2.2 BOTTOM-UP

Small organic molecules are pyrolyzed or carbonized as part of the "bottom-up" synthesis process. The four steps of CD creation are condensation, polymerization, carbonization, and passivation. First, a condensation reaction can be used to transform small organic molecule precursors into chain compound intermediates. Second, by covalent, non-covalent, or other interactions, the intermediaries are further polymerized. Third, at high temperatures, the polymers carbonize to create the carbon core. In order to increase the luminescence efficiency of CDs, leftover precursors can be changed to act as surface passivating agents [45].

Comparing the two methods above, even if top-down approaches are easy to use, it is very difficult to obtain scalability and proper particle size, for this reason often authors prefer to select bottom-up strategies [46].

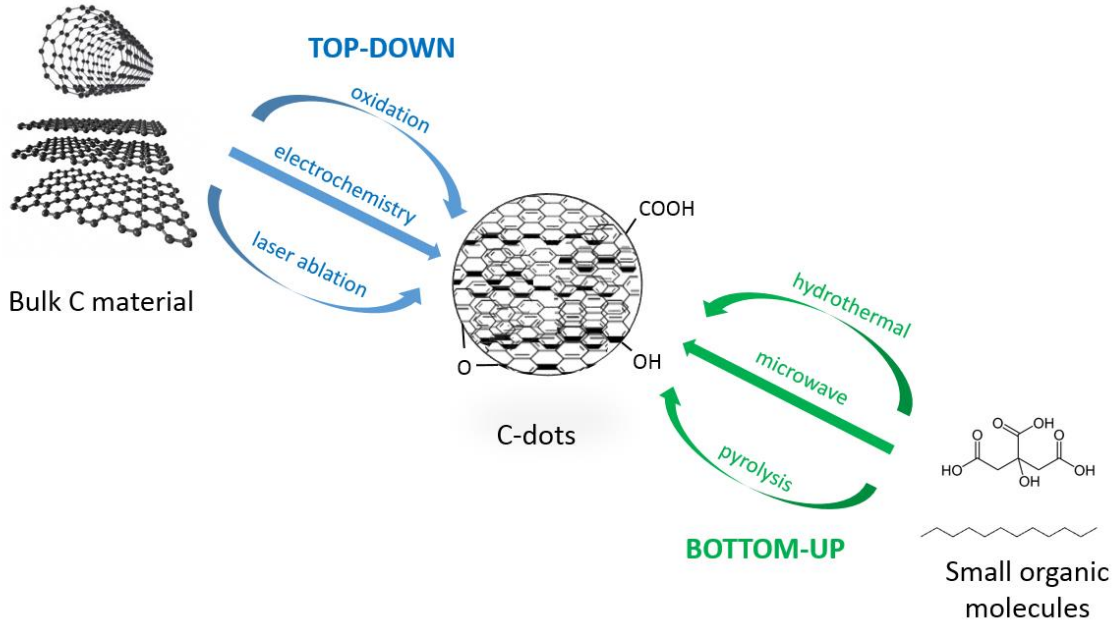


Fig. 1.9: Top-Down and Bottom-Up synthesis approach [42].

## 1.6.3 Classification

The classification of carbon dots is mainly based on the core structure, surface functional groups and main properties. They could be roughly classified into three main types based on their structural characteristics. These subcategories include polymer dots (PDs), carbon nanodots (CNDs), and graphene quantum dots (GQDs). Despite the differences in structure, size, and surface functional groups, all classes possess equivalent photoluminescence features. CNDs are mainly spherical and amorphous , GQDs are made up of a few layers of graphene with chemical groups on the edges and CNPs tend to present a crystalline structure [48]. Polymer dots can either be cross-linked/aggregated linear polymers or chains of polymer gathered around a sphere of carbon [48, 49].

### 1.6.4 Biological applications

Thanks to their size and surface functional groups that increase the possibilities of functionalization, C-dots have many healthcare applications. The most important ones include biosensors (both optical and electrochemical biosensing), bioimaging, drug delivery, gene transfer, and photothermal therapy [41].

In the field of biosensing, the research is focusing on finding some tools that can be easily reproducible, ultrasensitive, and specific for particular targets. Some examples include CDs functionalised with antibodies and applied for monitoring cardiovascular diseases as acute myocardial infarction; others have been synthetized with chitosan for electrochemical immunosensing. Also, optical biosensors play a central role in this field. [48,52].

In bioimaging, C-dots are used especially as contrast media for different imaging techniques such as positron emission tomography (PET), ultrasonic imaging, computed tomography imaging (CT), magnetic resonance imaging (MRI).

# CHAPTER 2
# PROJECT GOALS

The main goal of this work is the synthesis and analysis of fluorescent dysprosium-doped carbon dots that could be suitable for MR imaging and theranostic applications. The evolution and recent development of imaging techniques have brought MRI procedure to a higher level to adapt to the necessities of performing imaging exams in shorter times and with higher resolution. This can be done using a higher magnetic field: generally, normal MRI scans work in a range of 1.5-3 T, while the newest instrumentation can reach 7 T. Unluckily, the efficiency of the currently approved contrast agents, mainly gadolinium-based agents, decreases at higher magnetic fields. As mentioned before, the efficiency of a contrast agent depends on the relaxivity (r2/r1) where r1 is 1/T1 and r2 is 1/T2. The higher the relaxivity, the higher the efficiency of a T2 contrast agent (such as dysprosium) and vice versa for a T1 contrast agent (such as Gadolinium). In fact, recently, the dysprosium ion ($Dy^{3+}$) has been regarded as the finest choice for a contrast agent. This ion has a rapid relaxation time and a strong magnetic moment. Dysprosium could be especially helpful for imaging the bone marrow, liver, and spleen. The synthesized carbon dots should be appropriate for imaging at higher magnetic fields producing negative contrast MR images.

Carbon quantum dots have shown a passive uptake in tumors and retention effect too and their dysprosium-conjugated derivatives could be used as theranostic tools. This new approach opens the way to both personalized medicine and imaging-guided therapy. In this context, the previously prepared carbon nitride dots were conjugated to doxorubicin, a chemotherapeutic drug largely used for treating, among others, blood, bladder, breast, lungs, and nerve cancers.

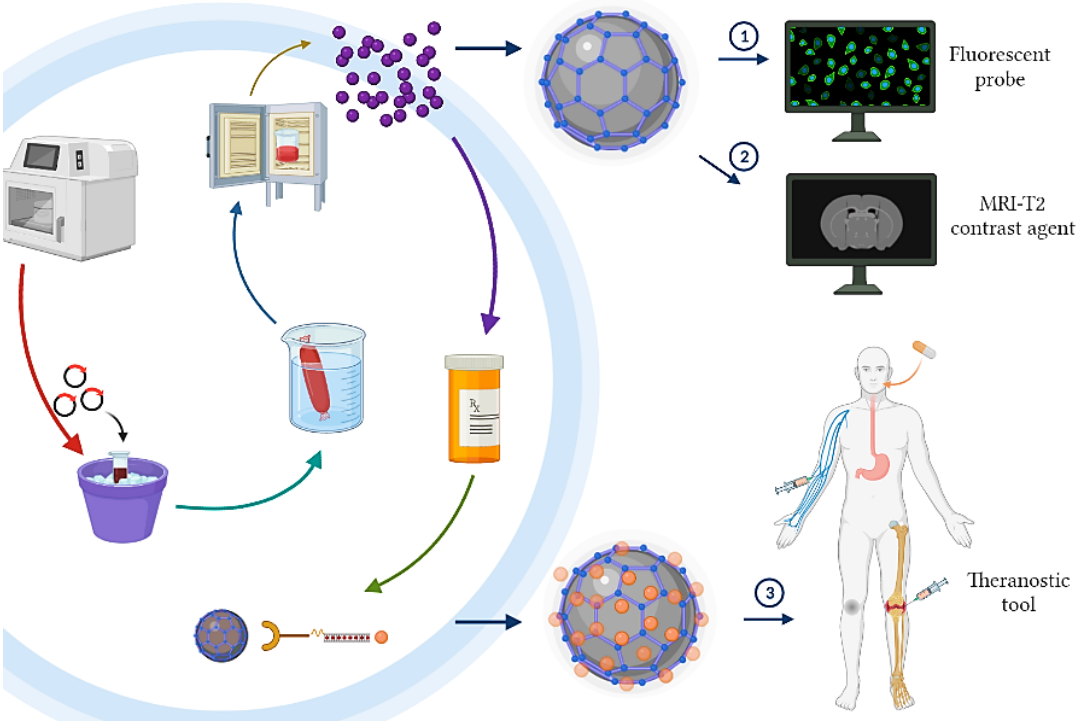


Fig. 2.1: Synthesis of dysprosium-doped C-dots suitable fluorescent probes, MRI-T2 contrast agents, theranostic tools after doxorubicin conjugation.

# CHAPTER 3
# MATERIALS AND METHODS

## 3.1 Materials

Citric acid, urea, and dysprosium chloride hexahydrate were bought from Sigma-Aldrich. Sodium Hydroxide pellet was acquired from Sigma-Aldrich too. The 0.2 μm filter membranes were obtained from Sterlitech. Doxorubicin was bought from Sigma-Aldrich. All chemicals were used without any purification. The instruments used for the synthesis and conjugations included an Agilent Cary 100 UV-vis spectrophotometer for UV-vis spectra acquisition, a Fluorog HORIBA Jobin Yvon fluoremeter for photoluminescence (PL) characterization, an FT-Nicolet 5700 FTIR spectrometer, a Malvern Zetasizer nano-series for the Zeta potential, a Veeco Metrology Multimode/Nanoscope IVA for AFM studies, a Vibra cell sonicator, hot plates with magnetic stirrers, an electronic balance, a domestic microwave. Plus, a Brucker EMNXNano bench instrument was used for EPR measurements, and a Netzsch TG 209 F3 Tarsus thermos-microbalance was used for TGA measurements.

## 3.2 Methods

First, a synthesis procedure was selected. We adopted a process that had already been tried by other authors. Then, some steps of the procedure were slightly modified. Once the product was ready for analysis, it was characterized to verify the formation of the carbon dots and assess the main problems. Using this method, it was possible to improve the synthesis procedure and optimize the various steps. It is important to highlight the fact that synthesis and characterization were done in parallel to grant better results. This approach increased the possibility to improve the work and be consistent through the different steps. After the synthesis and preliminary characterizations, an EDC/NHS mediated coupling process was applied to conjugate doxorubicin to the previously prepared carbon dots. After the conjugation, C-dots were characterized. Finally, additional analyses were conducted including the study of relaxometric properties and cellular tests.

### 3.2.1 Synthesis

Two main approaches were adopted to synthetize the C-dots. The hydrothermal synthesis and microwave-mediated method were considered.

As mentioned before, the synthesis procedure was selected from literature, from the work of Piumi et al [51]. However, a few steps were changed and adapted to the needs of the project.

The selected synthesis consisted of a microwave-mediated procedure. The chemicals were dissolved in 25 mL of deionized water (DI) and the solution was stirred overnight. Then the mixture was poured into a 250 ml Erlenmeyer flask and then put into a microwave oven (power of 700W, total time of 7 minutes). Once the water was evaporated, the remaining part was collected, dispersed in 15 mL of deionized water, and sonicated for 30 minutes. The resulting solution was centrifuged twice for 30 minutes at 3000 rpm to remove larger particles. Then, the solution was filtered through a 0.2 μm filter membrane. The filtrate part was dialyzed in a 100–500 Da MW cutoff dialysis membrane for 3 days in deionized water and the water was changed every 24 hours. For the drying step, two different methodologies were

adopted and will be further explained. The first one consisted of evaporating the solvent using a rotovap reaching 70–80 °C and then putting the resulting part in a laboratory oven overnight. An alternative drying method consisted of freezing the dialyzed solution overnight and then lyophilizing it for at least 3 days.

Citric acid and dysprosium chloride hexahydrate were precursors in each set. The same synthesis method was followed for the precursors set that included urea.

The main synthesis that will be mentioned here was investigated using different ratios that were analyzed to understand the reactivity and the main requirements that derived from the use of the selected precursors, in particular dysprosium chloride.

### 3.2.2 Purification

The internal composition of carbon dots is largely debated. It is also hypothesized the presence of molecular intermediates and side products, after the synthesis of carbon dots. For this reason, a few steps of purification are needed to extrapolate the CD fraction of interest [52].

After the carbonization, the prepared carbon dots needed to go through some steps of purification. Different methods were implemented to find out the best alternative.

The selected process for the preliminary purification included a NaOH filtration for the removal of unreacted particles and a further step of centrifugation.

First, a highly concentrated NaOH solution was prepared. The prepared carbon dots were washed with it and then filtered with vacuum filtration to remove the unreacted residues and salts. Then, two rounds of centrifuge were applied (3000 rpm, 30 minutes each).

A further step of purification by dialysis was applied. For the purposes of the project and considering the molecular weight of the prepared carbon dots, 500 Da cutoff dialysis membranes were selected. The purpose of this part was to remove smaller particles, with a molecular weight lower than 500 Da.

It is important to mention that the dialysis membranes were designed for the purification of proteins and then their use was extended to carbon dots. This type of purification works for the purpose of this work, but it can present some defects too.

The carbon dots were kept in dialysis in water for three days, changing the water every 24 hours to grant the process of osmosis and the removal of all the undesired particles.

### 3.2.3 Optimization process

During the step of the synthesis, an optimization process was implemented. The method that was adopted consisted of varying just one parameter at a time and keeping the others constant. In this way, it was possible to evaluate which parameters improved the characteristics of the carbon dots. In the next paragraph, the optimization process will be explained in detail.

In Table 2, the main synthesis are reported. The parameters that were modified included mainly the ratio and concentration of precursors, the carbonization method, the drying method, and the purification process.

First, the ratio was varied to find the best one for the preparation of the carbon dots. An initial 12 ratio based on previous work on Gadolinium chloride was adopted (0.5 g of dysprosium chloride hexahydrate and 1 g of citric acid). The properties of these carbon dots were not optimal: through Atomic Force Microscopy, it was stated that the dimension was not homogenous and that probably there were clusters of particles. After, a ratio of 11 was applied (0.5 g of dysprosium chloride hexahydrate and 0.5 g of citric acid) but the properties were even worse. For this reason, based on the work of other authors, the quantity of dysprosium was lowered (0.25 g of dysprosium chloride hexahydrate and 0.5 g of citric acid). The lowered concentration of precursors helped to improve the step of carbonization.

Then, the carbonization process was analysed. It was adopted a microwave-mediated method synthesis process. Later, it was discussed the efficacy of this process. For this reason, it was tried an autoclave mediated carbonization process. The obtained result was not good as expected. Probably because of the insufficient time inside the autoclave, the C-dots did not form. This was stated through the fluorescence emission of C-dots. By irradiating the solution with UV light no fluorescence was detected. Then, the characterization of the optical properties confirmed this hypothesis.

| ***C-DOTS SYNTHESIS: OPTIMIZATION PROCESS*** | | | | | | |
|---|---|---|---|---|---|---|
| RATIO | CDs 11 | CDs 12 | CDs 14 | CNDs 111 | CNDs 122 | CNDs 112 |
| CONCENTRATION OF PRECURSORS | Higher concentration | | | Lower concentration | | |
| CARBONIZATION METHOD | Autoclave | | | Microwave | | |
| DRYING METHOD | Oven | | | Lyophilizer | | |
| FILTRATION | Type of filter and number of filtrations | | Centrifuge parameters | | Purification with NaOH | |

Table 3.1: Parameters varied for the optimization of Dysprosium Carbon Dots Synthesis

### 3.2.4 Conjugation

Doxorubicin was the selected drug for conjugation. This pharmaceutical is largely used for treating different types of cancers including breast, bladder, lung, nerves cancers. For this project, doxorubicin was preferred to other drugs, such as gemcitabine. The reason was that the success of the conjugation could have been easily assessed evaluating the fluorescence after coupling doxorubicin on the C-dots.

The selected conjugation process was a EDC/NHS mediated coupling to form a carbodiimide. EDC activates DyCNDs' COOH groups producing an O-acylisourea intermediate. This intermediate reacts with primary amines, forming an amide bond [53,54].

Before starting the conjugation, the number of carboxyl groups was assessed through titration. The titration was conducted with a NaOH solution. It was found that the DyCNDs had the highest number of carboxyl groups, for this reason, the conjugation was conducted on this type of C-dots, increasing the chances of realizing a successful coupling. The higher number of carboxyl groups was probably due to the fact that urea, during the carbonization process, exposes a high number of COOH groups on the surface.

Through titration, it was assessed that 10 mg of DyCNDs are characterized approximately by 9,8 μmols of carboxyl groups. Considering the molecular masses of EDC (191,7 g/mol)and NHS (115,1 g/mol) and adopting a ratio of 1:2 for both the precursors, 3,8 mg of EDC and 2,3 mg of NHS were used for the conjugation. Assuming a ratio 1:1 for Doxorubicin (543,2 g/mol), 5,3 mg were taken.

The process consisted of diluting 10 mg of DyCNDs in 3 ml of PBS, then 3,8 mg of EDC were added, and the solution was stirred for 30 minutes. After, 2,3 mg of NHS were added to the mixture and stirred for 30 minutes. Finally, 5,3 mg of doxorubicin were added, and the solution was stirred overnight. A few ml of PBS were poured in each step to grant the dilution of the component. However, the volume of the solution was kept low to enhance the reaction of the precursors, increasing the probability of a successful conjugation. The solution was not exposed to light, considering that doxorubicin is light and heat sensitive.

After 24 hours, the mixture was put in a dialysis bag cutoff 1000 Da and dialysed in water for 5 days, making sure all the unreacted particles were expelled. Finally, the mixture was freeze-dried.

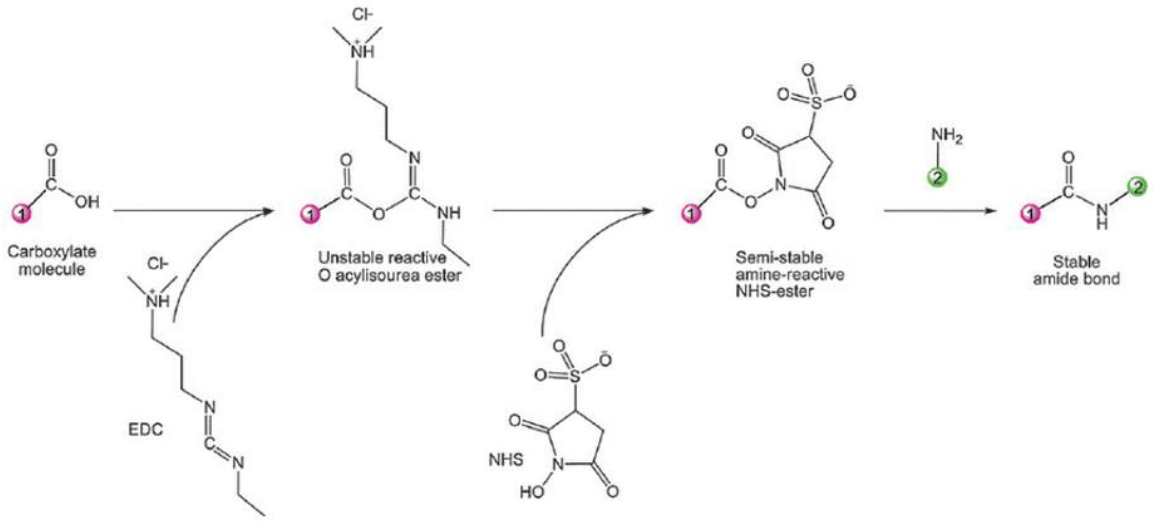


Fig. 3.1*:* EDC/NHS coupling mechanism [55].

## 3.2.5 Characterization

As mentioned above, synthesis and characterization were conducted in parallel to optimize the process. Characterization included a first step that was repeated constantly after each synthesis to assess the optical properties through UV-Vis, fluorescence, FT-IR spectroscopy.

Then, if the results of this preliminary characterization were acceptable, the CDs were further analysed through AFM to evaluate the dimension, Zeta Potential, MALDI-TOF to assess the atomic mass, TGA to study the composition of the carbon dots.

## 3.2.6 Tests

This section consisted mainly of cellular tests and EPR experiments.

EPR was conducted to study the ground-state properties of the particles.

The goal of cellular tests included studying the viability of the cells after the interaction with the dysprosium doped-CDs and their fluorescence.

### 3.2.6.1 ELECTRON PARAMAGNETIC RESONANCE SPECTROSCOPY

The EPR analysis was conducted with a Bruker Elexsys 580 EPR spectrometer, operating in X band. The powdered samples were inserted in quartz tubes of 2 mm inner diameter. The tests were conducted at room temperature.

### 3.2.6.2 CELL VIABILITY STUDIES

SKN-AS, SKN-BE2C (neuroblastoma cell lines), MSC (mesenchymal stem cells) and VSMC (vascular smooth muscle cells) were selected for viability studies. RPMI-1640 media (ThermoFisher Scientific, Waltham, MA, U.S.A.) was used to culture all cell lines. 10% fetal bovine serum (FBS) and 1% penicillin/streptomycin (both from Gemini Biosciences, West Sacramento, CA) were added to the media and incubated at 37 °C in humidified 5% CO2. Cell viability was determined by using the CellTiter 96 AQueous One Solution Cell Proliferation Assay (MTS) (Promega Madison, WI). MTS assay was applied after 72 h of incubation [46].

### 3.2.6.3 STATISTICAL ANALYSIS

A statistical analysis was conducted on cellular tests results using ANOVA. The analysis was implemented through Excel. Values were considered statistically significant for $p<0.05$.

### 3.2.6.4 CELLULAR IMAGING

In this work, SK-N-BE2C neuroblastoma cells were further analyzed with cellular imaging tests. The cell line was treated with 50 g/mL DyCNDs and incubated for 24 hours before being imaged with a fluorescent microscope. DyCNDs were employed for imaging because of the higher fluorescence emission and good cellular viability rates. Plus, DyCNDs were selected in view of future tests on DyCNDs conjugated with doxorubicin.

# CHAPTER 4
# RESULTS AND DISCUSSION

## 4.1 C-DOTS

As previously mentioned, every set of C-dots was produced using a one-pot method starting from two precursors for the CDs (Citric Acid and Dysprosium Chloride Hexahydrate) and three precursors for the carbon nitride dots (CNDs) adding urea to the previous two. The following images show the three precursors.

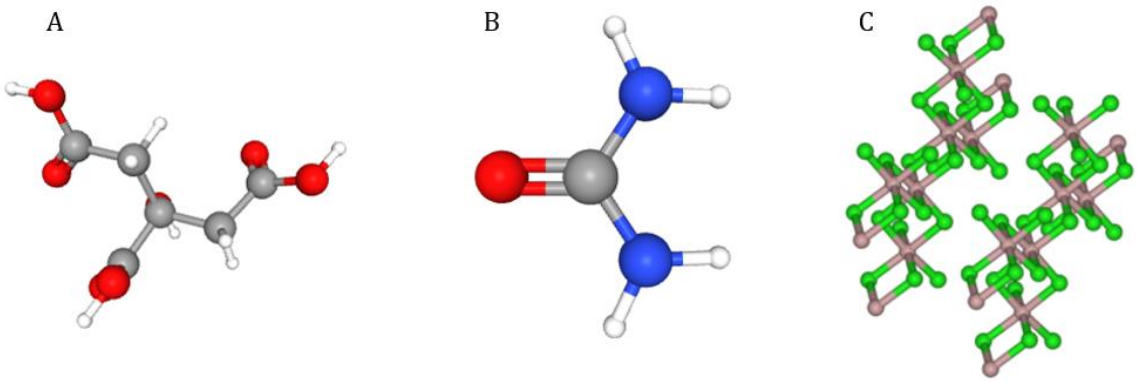


Fig. 4.1 : Synthesis precursors. A) Citric acid, B) Urea, C) Dysprosium chloride hexahydrate.

The process followed for the synthesis of the carbon dots is the one presented in the work of Piumi et al. [51] in which CNDs are investigated as a selective imaging biomaterial. The synthesis steps were slightly modified for the purposes of this project.

### 4.1.1 MECHANISM OF FORMATION

As mentioned before, two main classes of carbon dots have been synthesized: carbon dots from citric acid and dysprosium precursor and carbon nitride dots, in which urea was employed as a nitrogen source. Typically, urea and N-rich precursors have been used to create carbon nitride dots [51]. In literature [46], different synthetic methods have been adopted, such as the solvothermal method, electrochemical method, pyrolysis, and chemical oxidation. However, these syntheses show some inherent limitations, such as the need for high-temperature treatments and particular instrumentation. Additionally, some of the produced materials have large particle sizes, which result in poor photoluminescent (PL) properties. Due to its vast abundance, low cost, and high activity under thermal

treatment, urea has been a particularly attractive N-rich precursor for the synthesis of CNDs. Concerning the use of citric acid, this precursor is fundamental for the formation of C-dots because of its high abundance of carboxylic groups.

The selected preparation process is a one-step microwave-mediated synthesis method. This choice is due to the fact that it is simpler to operate and has faster heating rates than traditional heating techniques (such as the autoclave method).

The preparation of the carbon dots included the use of dysprosium chloride hexahydrate too.

The preparation of the CDs and CNDs was conducted using the same protocol. The main difference was the addition of urea for the preparation of the CNDs. Tri-s-triazine rings are an important component in the majority of carbon nitride nanomaterials. In this case, a bottom-up synthesis method that included the use of a N-rich precursor was adopted to create the CNDs. Citric acid was used in all the synthesis to boost the amount of carboxylic functional groups on the surface of the carbon dots.

By using MALDI-TOF mass spectrometry, it was determined that the CDs and CNDs' molecular mass was around 600 Da. As a result, the purification process employed a 100–500 Da molecular weight cutoff dialysis membrane.

Despite the high variety of characterization techniques, the internal structure of the C-dots and their mechanism of formation is still not clear. The most likely scenario is the formation of a luminescent carbon dot with a gradient component of dysprosium. Indeed, a one-pot synthesis was preferred to a two-step method mainly because of a concern about the interaction of the dysprosium with the carbon dot. The two-step method included a first phase of synthesis of the carbon dot and a second phase of functionalization with the dysprosium. This approach was rejected because most of the dysprosium would have been exposed on the surface of the particle, possibly increasing the cytotoxicity of the carbon dots. For this reason, it was preferred a one-pot method, increasing the dysprosium inside the carbon dot and hypothetically reducing its toxicity. In Fig. 4.2, it is reported the proposed gradient model. However, further analysis is needed to evaluate the validity of this model.

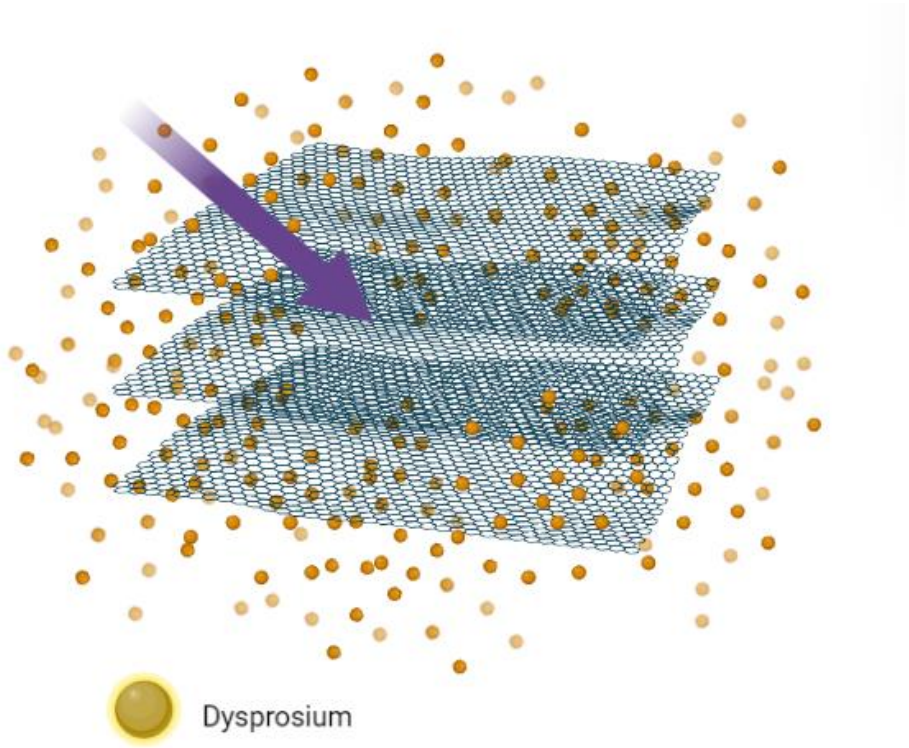


Fig. 4.2 : Proposed gradient model of dysprosium carbon dots. Dysprosium possibly penetrates between the graphene planes of the CD.

## 4.2 CHARACTERIZATION AND TESTS

### 4.2.1 UV-vis Spectroscopy

Spectroscopic techniques are based on the energy exchange that occurs between radiant energy and matter. Absorption spectrophotometry is interested in the absorption phenomena of light radiation in the region of the electromagnetic spectrum belonging to the visible range (350 - 700 nm) and near ultraviolet (200 - 350 nm). Absorption of these types of radiation by molecules produces energy transitions of both sigma and pi electrons. The first ones (sigma (σ) type) consist of an electron cloud distributed along the bond axis; pi type are electron pairs whose density is located outside the bond axis (such as in double and triple bonds). Pi (π) electrons are more easily excited than sigma (σ) electrons [47]. Since each substance has its own absorption spectrum, the study of the spectra makes it possible to identify a particular substance by direct comparison with known samples or through spectra databases.

In this work, each set of C-Dots was analyzed to obtain the absorption spectrum. The range of interest goes from 800nm to 200nm. Observing the dysprosium C-dots spectrum, it is possible to notice two main peaks. These two peaks are characteristics of absorption spectra of carbon dots, and they are useful to prove the formation of these particles. Generally, the two regions of interest are from 200 to 300 nm and from 300 to 400 nm. The first region includes peaks associated with the π-π* transition of

CC bonds and sp2 planes, while the second one is associated with the n-π* transition of CO and CN groups. For Dy-CDs, the optical absorption peaks were observed at 251 nm and 348 nm, while for Dy-CNDs at 346 nm and 399 nm. It is important to highlight the differences between carbon dots and carbon nitride dots: for the CNDs it is evident that the peaks in the region from 300 to 400 nm are higher, probably because of the presence of urea [47]. In this region, the absorption bands can be due to the presence of nitrogen atoms inside the structure of carbon dots.

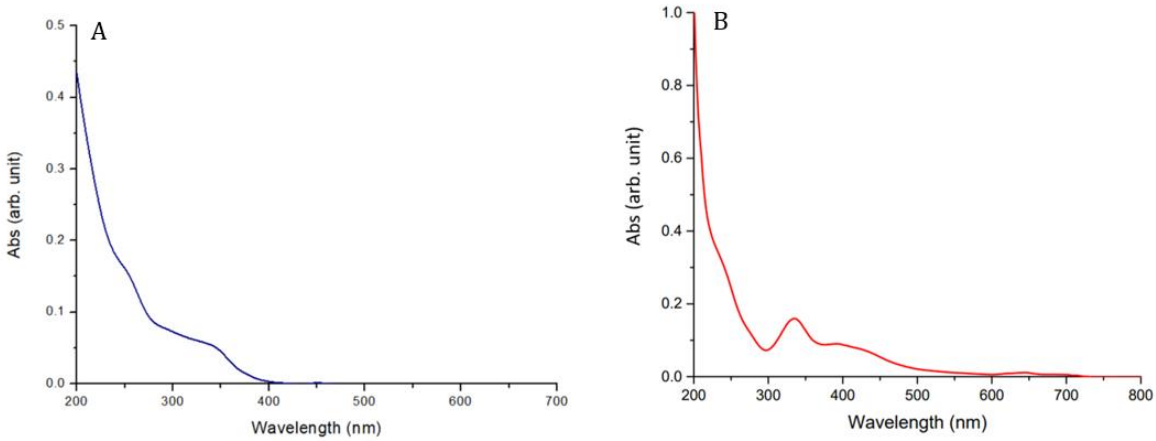


Fig.4.3: Absorption UV-Vis spectrum of DyCDs (left) and DyCNDs (right). The concentration was 0,1 mg/ml for both solutions.

The photoluminescence usually depends on the emission wavelength and size of the C-dots. When exposed to UV light, the synthesized carbon dots in an aqueous solution emit in the blue range, as seen in Fig. 4.4. As expected, the photoluminescence of the solution depends on the concentration of the solution itself: the higher the quantity of C-dots, the more intense the photoluminescence. At low concentrations, there may be a decrease in interactions between the various polar groups [58].

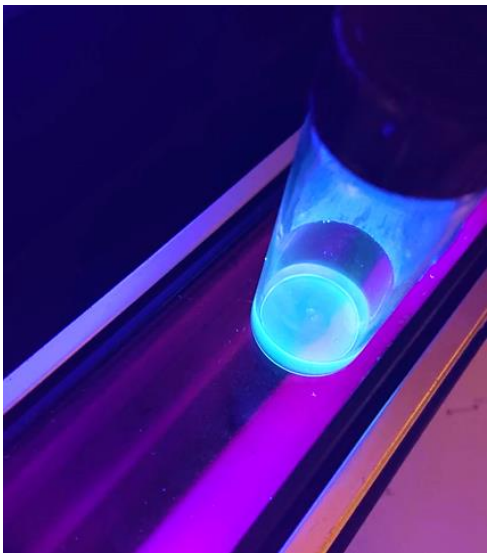

Fig. 4.4: Blue emission of DyCNDs using a wavelength of 320 nm.

### 4.2.2 Fourier-Transform Infrared Spectroscopy (FT-IR)

FT-IR spectroscopy has been conducted on both Dy-CDs and Dy-CNDs samples. This technique helps to find out the functional groups present on the surface of C-Dots. The results are very similar for the three samples. From the felt, the first peak (respectively, 3305 $cm^{-1}$, 3291 $cm^{-1}$, 3478 $cm^{-1}$) is associated with the stretching vibrations of hydroxyl groups. DyCNDs show a N-H stretching at 3200 $cm^{-1}$. The peak at 1695 $cm^{-1}$, 1693 $cm^{-1}$ and 1773 $cm^{-1}$ can be associated with the C=O stretching vibration. C=C stretching in the aromatic ring can be noticed at 1552 $cm^{-1}$, 1563 $cm^{-1}$ and 1659 $cm^{-1}$. The bands at 1071 $cm^{-1}$, 1080 $cm^{-1}$ and 1097 $cm^{-1}$ represent a C-O-C stretching, while the ones at 764 $cm^{-1}$,767 $cm^{-1}$ and 778 $cm^{-1}$ refer to a C-H bending.

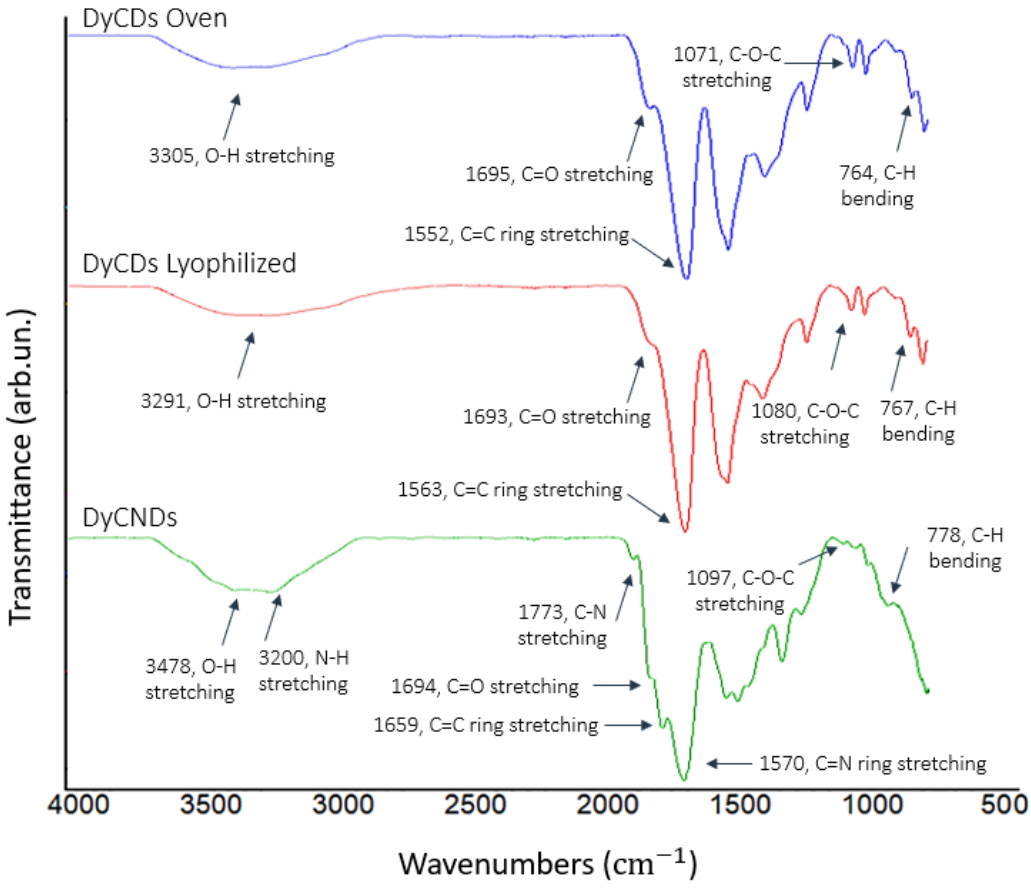


Fig. 4.5: IR spectra of DyCDs Oven, DyCDs Lyophilized and DyCNDs.

No relevant differences between the oven dried C-dots and lyophilized ones are reported. On the contrary, the carbon nitride dots show some diverse peaks due to the presence of nitrogen bonds. DyCNDs show a N-H stretching at 3200 $cm^{-1}$ and a C=N ring stretching at 1570 $cm^{-1}$.

From the FT-IR analysis, it is stated the presence of oxygen-rich groups including hydroxyl, carboxyl, and carbonyl on the surface of carbon dots. The formation of these surface residues is consistent with the hydrothermal technique used to create carbon dots [47]. Plus, the presence of these functional groups can explain the water-soluble character of the prepared carbon dots.

| DyCDs Oven | | DyCDs Lyophilized | | DyCNDs | |
|---|---|---|---|---|---|
| 3305 | O-H stretching | 3291 | O-H stretching | 3478 | O-H stretching |
| 1695 | C=O stretching | 1693 | C=O stretching | 3200 | N-H stretching |
| 1552 | C=C ring stretching | 1563 | C=C ring stretching | 1773 | C=O stretching |
| 1071 | C-O-C stretching | 1080 | C-O-C stretching | 1694 | C-N stretching |
| 764 | C-H bending | 767 | C-H bending | 1659 | C=C ring stretching |
| | | | | 1570 | C=N ring stretching |
| | | | | 1097 | C-O-C stretching |
| | | | | 778 | C-H bending |

Table 4.1: Wavenumbers ($cm^{-1}$) and type of C-dots' IR spectra peaks.

### 4.2.3 Fluorescence Spectroscopy

Carbon dots (CDs) are well known for their fluorescent properties. A lot of applications exploit the photoluminescence of CDs [60].

Fluorescence spectroscopy was conducted on both DyCDs and DyCNDs with excitation wavelengths from 320nm (4.25eV) to 420nm (3.24eV). The concentration of each sample was 0.05 μg/ml. Fig. 4.6 to 4.11 show the fluorescence spectra of the prepared C-dots.

All the CDs show strong blue fluorescence emission. The emission band lies mainly from 340 to 550 nm. The shape of the peak remains unchanged, while the intensity varies according to the excitation wavelength. From 380 nm (excitation wavelength), there is a progressive reduction in intensity. For both samples, the highest peak is around 450 nm (453nm for the CDs and 446 for the CNDs) and it is associated with an excitation wavelength of 360 nm when the CDs are excited in the n–π* absorption band.

From the fluorescence spectra, it is possible to state that the prepared carbon dots show excitation-dependent and red-shifted emission properties.

The first main difference between fluorescence spectra of CDs and CNDs is the higher intensity of CNDs emission compared to the one of CDs. In fact, it is largely known that the presence of urea enhances fluorescence intensity [61].

Tunable photoluminescence and excitation-wavelength-dependent emission are displayed using carbon dots (CDs). Fluorescence's color is influenced by local fluorophores, surface defect states, conjugated -domain electronic bandgap transitions, and element doping [60].

The quantum confinement effect (QCE) is a crucial feature of CDs. When the material's three-dimensional size is reduced to the nanometer level, the valence band and conduction band pass from continuous energy bands to discrete energy levels, and the band gap widens. This causes a band gap transition in the ultraviolet-visible region and significantly boosts the fluorescent quantum yield (QY) [60].

For many carbon dots, fluorescence originates from the QCE. This happens especially for CDs with large π-domains: the band gap is smaller, and the emission peak is redshifted [60]. Fluorescence mechanism could be due to the presence of surface defects too. When the CD is excited with light, photons gather in the nearby surface defects. They will then return to the ground state to emit visible light of various wavelengths. The amount of surface oxidation on CDs increases with surface flaws and emission sites, which causes the emission wavelength to shift toward the red [60,62]. Doping the CDs with other elements can change surface properties by adding new surface functional groups or altering the original band gap [60,63].

FT-IR spectroscopy assessed the presence of hydroxyl and carboxyl functional groups that could be associated with trap states and defects. The presence of an inhomogeneous surface state could explain the excitation dependent emission behavior of the carbon dots [63].

The energy plots (Fig. 4.8 and Fig 4.11) show new insight into the fluorescence of the prepared CDs. From these plots, we can hypothesize the presence of a broad band that provides a spectrum with multiple peaks when excited at its ends. In fact, the energy plots show a single peak for DyCDs at an excitation wavelength of 400 nm and for DyCNDs at an excitation wavelength of 320 nm.

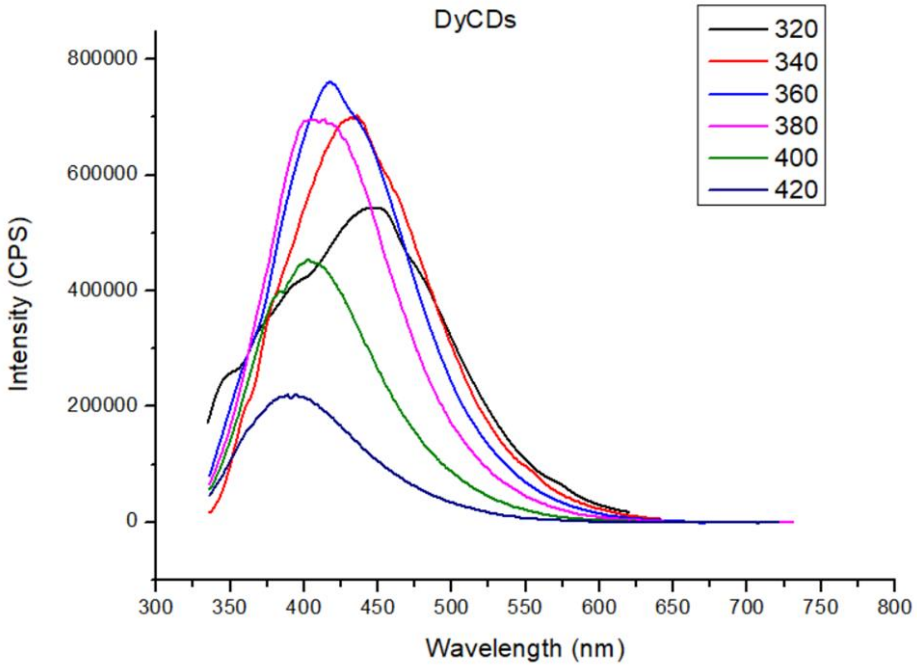


Fig. 4.6: Fluorescence spectrum of DyCDs.

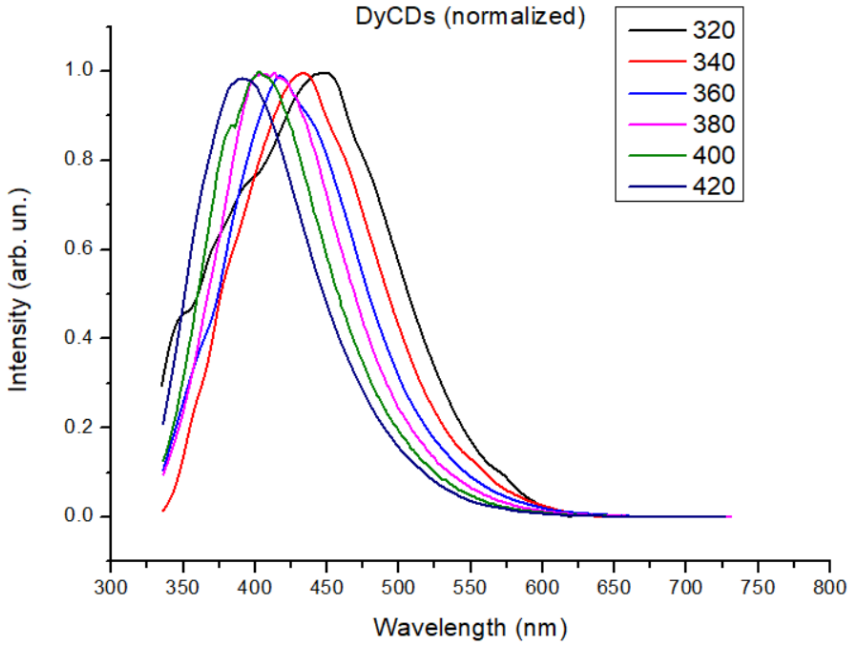


Fig. 4.7: Normalized fluorescence spectrum of DyCDs.

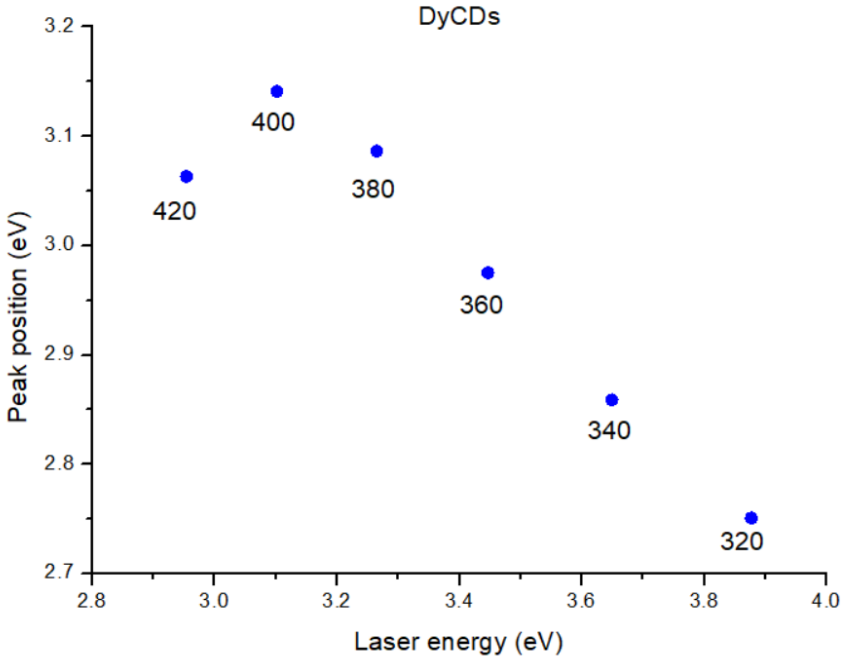


Fig. 4.8: Energy plot of DyCDs.

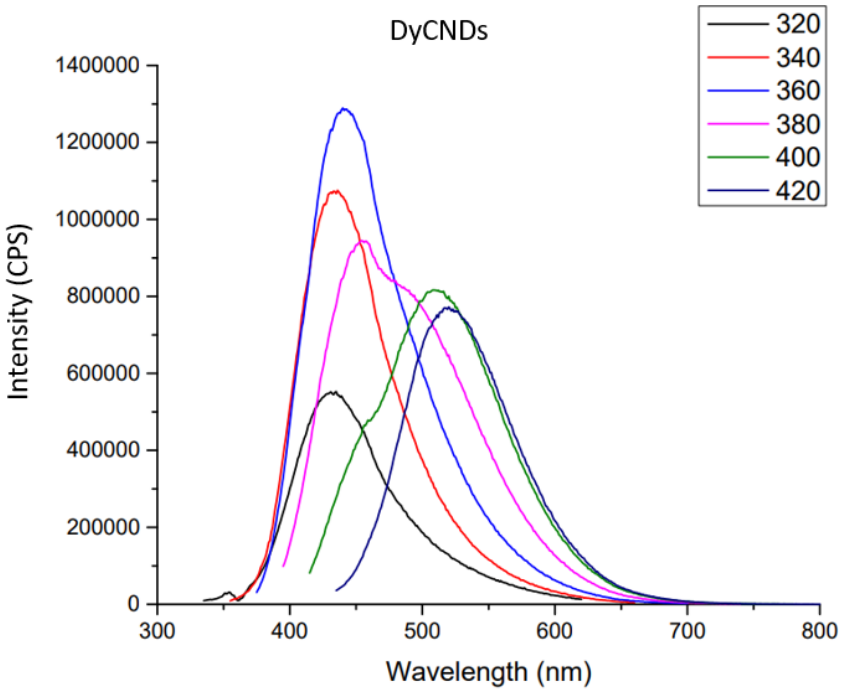


Fig. 4.9: Fluorescence spectrum of DyCNDs.

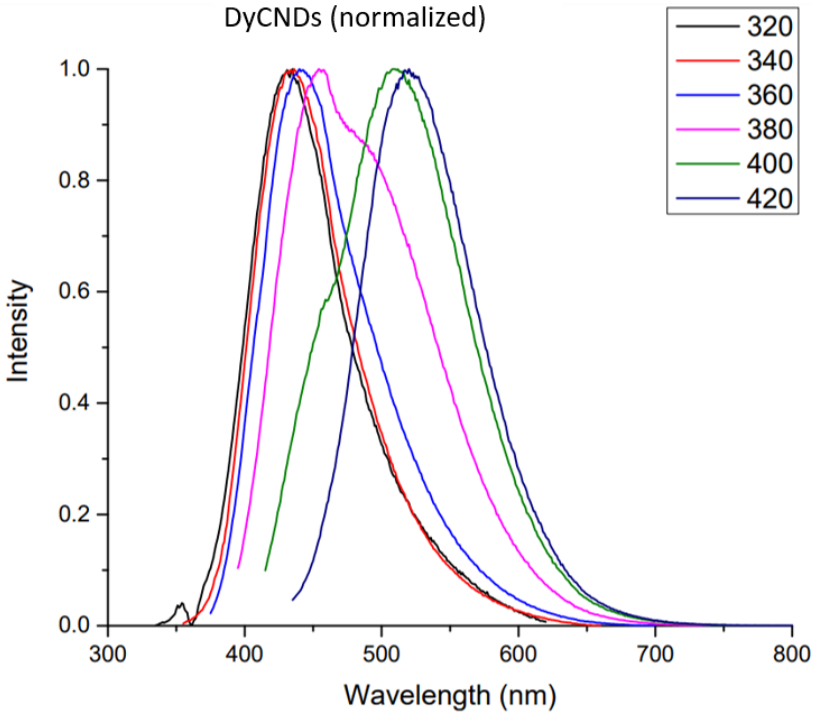


Fig. 4.10: Normalized fluorescence spectrum of DyCNDs.

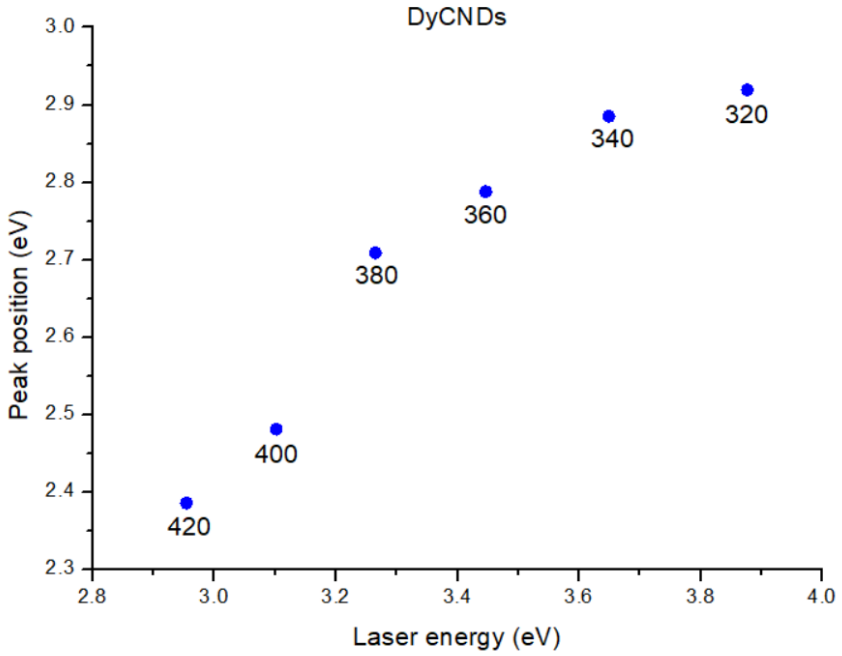


Fig. 4.11: Energy plot of DyCNDs.

### 4.2.4 Atomic Force Microscopy

Unlike the Scanning Electron Microscopy, which provides a two-dimensional projection or image of a sample, the AFM provides a three-dimensional surface profile. This is the reason why this type of characterization is fundamental for the C-dots [59]. In Fig. 4.12 and 4.13, both DyCDs and DyCNDs results are reported. The goal is synthetizing dimensionally homogenous carbon dots avoiding clusters formation. 2D and 3D AFM plots are reported, providing insights into the morphological structure of the particles. AFM images prove that the prepared CDs are rounded particles with a diameter of 2–10 nm.

Fig. 4.12 and Fig. 4.23 show C-dots' AFM results. The dimension of DyCDs is around 3.08 nm while the one of DyCNDs is about 3.69 and the distribution of is quite homogenous. Plus, no clusters are detected here.

Through AFM images, it was assessed that the prepared particles can be classified as carbon dots.

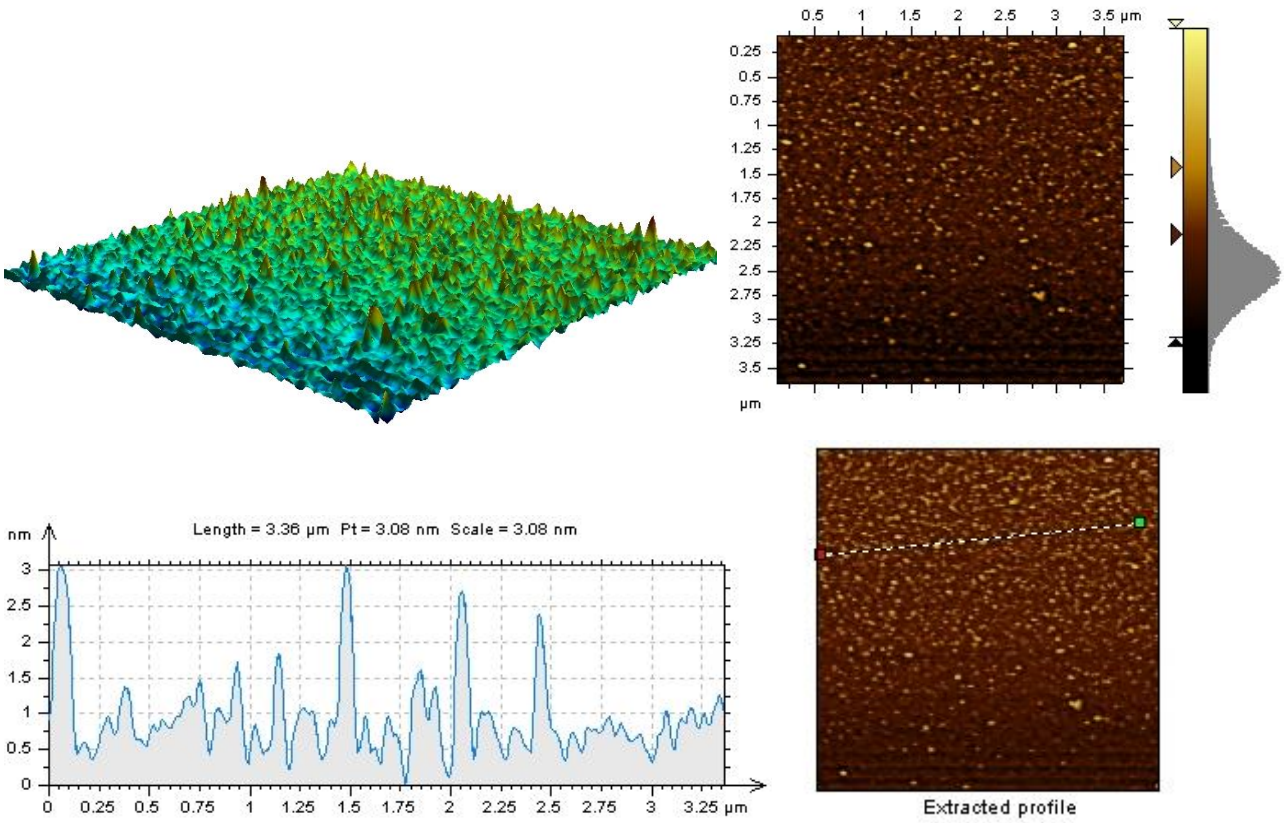


Fig. 4.12: AFM images of DyCDs.

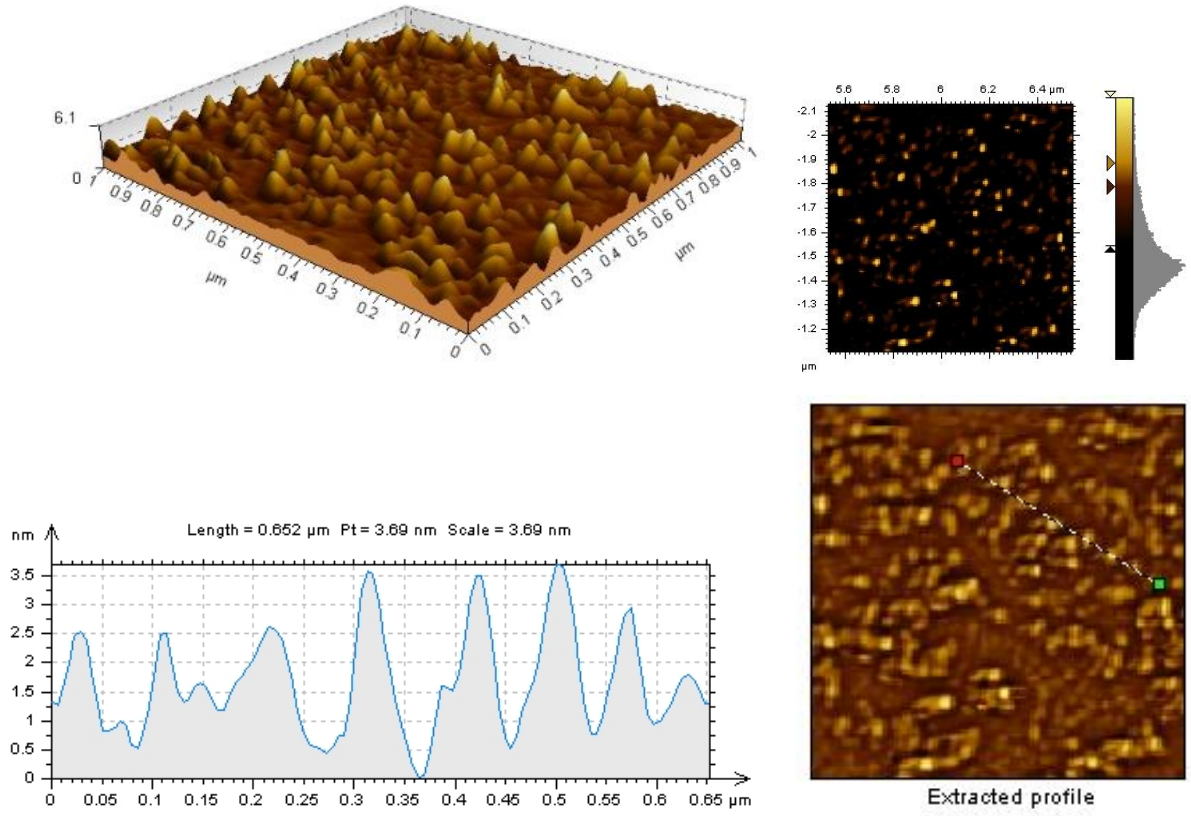


Fig. 4.13: AFM images of DyCNDs.

## 4.2.5 Zeta potential

A zetasizer was used to measure the zeta potential of the prepared C-dots. Additionally, this method could underline other characteristics of CDs, such as their hydrophilic functional groups (hydroxyl, carboxyl, and carbonyl). Usually, zeta potential measurements are a practical and effective way to assess the capacity of carbon dots to absorb heavy metal ions [54]. However, for the purposes of this project, zeta potential was an important factor to evaluate for the colloidal stability of the solution of CDs. In fact, carbon dots have to be suspended in an aqueous solution for their application as contrast agents. The measured zeta potential was 0.802 mV for DyCNDs, -0.503 mV for DyCDs dried in the oven and -0.705 mV for lyophilized DyCDs.

From literature [53], it is known that when the absolute value of zeta potential is higher (usually more than 30mV or less than -30mV), the repulsive forces tend to be stronger than the attraction forces, creating a system that is relatively stable. A zeta potential that lies in the range ± 10mV suggests that the studied particles are neutral, such as in this case. However, it is important to mention that the zeta potential is extremely susceptible to changes in dilution, pH, and ionic strength [53]. Therefore, further tests are needed to evaluate if there is a coalescence of the solubilized nanoparticles.

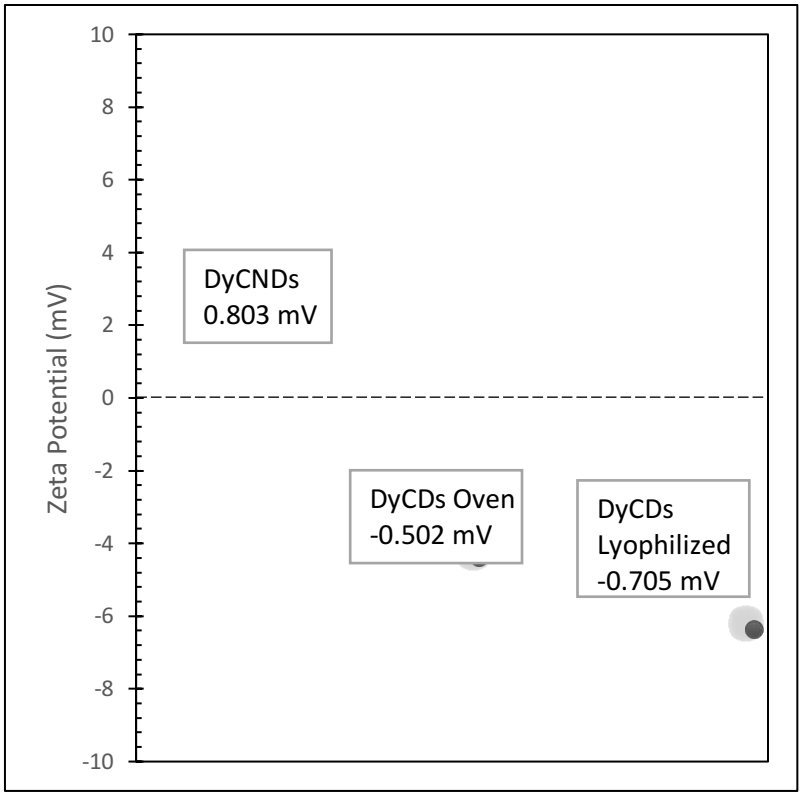


Fig. 4.14: Zeta potential of the three samples.

## 4.2.6 Thermogravimetric analysis (TGA)

The acronym TGA, Thermogravimetric Analysis, measures weight changes in a material when it is subjected to a gradual increase in temperature. Thus, TGA allows a quantitative analysis of the composition of a sample, but without directly identifying the nature of the components. TGA was conducted on three samples, DyCDs dried in the oven (Fig.4.15), DyCDs lyophilized (Fig.4.16) and DyCNDs (Fig. 4.17). The samples are heated from 30 to 300 degrees with an increment of 10 degrees per minute in an inert atmosphere. Increasing the temperature, chemical bonds are broken.

For the three samples, there is a first mass change due to the evaporation of water molecules adsorbed on the surface (respectively -5.71% for DyCDs Oven, -4.58% for DyCDs Lyophilized and -8.56% for DyCNDs). For DyCDs lyophilized, Fig. 4.16 shows a mass change of -2.15% due to -OH bonds. To note, the temperature reached in this first step is higher than 100 °C mainly because of kinetic effects. The mass change caused by the decomposition of carbonyl and carboxyl bonds is -17.06% for DyCDs Oven, -16.81% for DyCDs Lyophilized and -30.06% for DyCNDs. From these data, it is reasonable to hypothesize a stronger presence of -COOH groups in DyCNDs. The decomposition of nitrogen-containing bonds only takes place in the DyCNDs, due to the presence of urea in the precursors set.

The main difference between the lyophilized Dy-CDs and the ones dried in the oven lies in the quantity of -CO, -COOH and -OH bonds. The CDs dried in the oven go through further crystallization during the drying phase. CDs dried in the oven show higher quantities of -OH and -COOH groups because of the dismutation process. The dismutation is an oxidation-reduction reaction in which a chemical element transforms to one species in which it has a higher oxidation number and another in which it has a lower oxidation number. It is the case of the -CO groups of the oven-dried DyCDs that are converted to -OH and -COOH groups.

The final mass loss could originate from the decomposition of oxidized sp2 planes of the CDs. At the end of the analysis, the remaining part is constituted by the graphitic core with dysprosium [52].

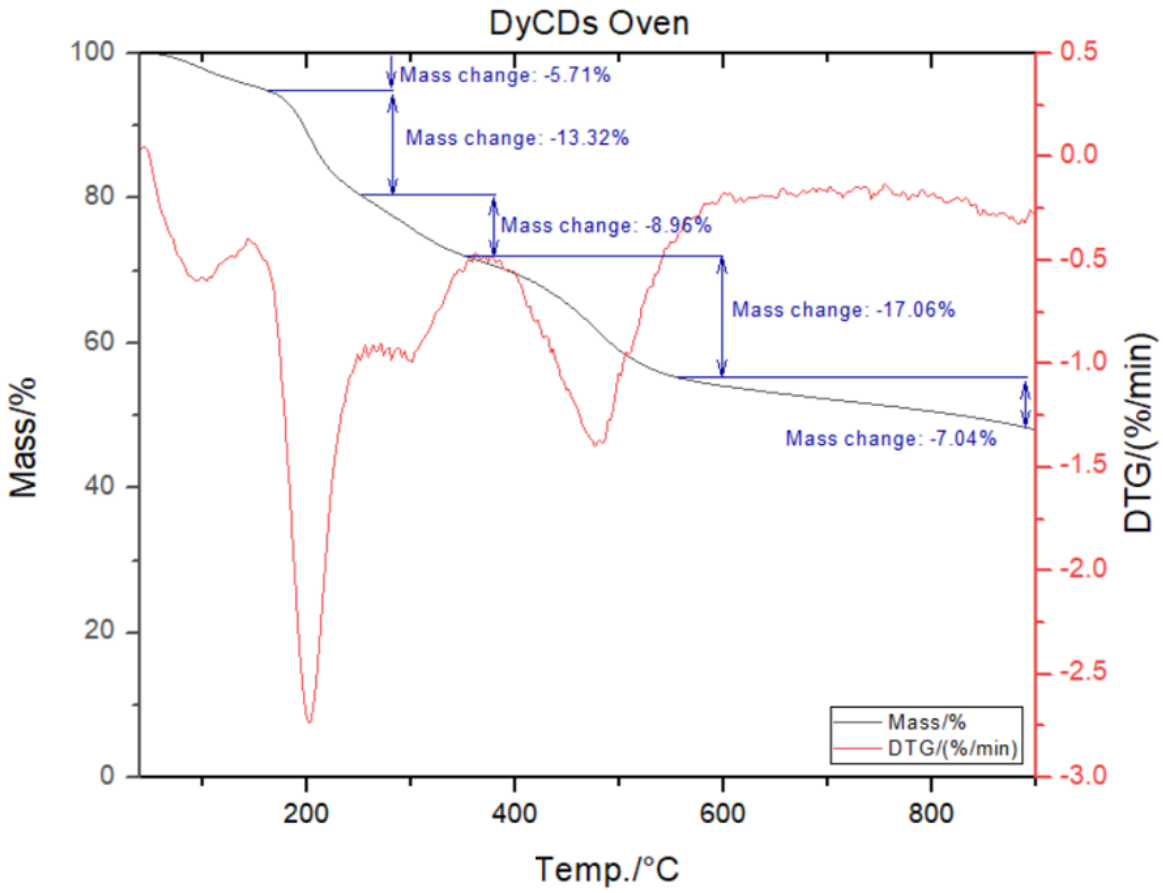


Fig. 4.15: TGA of DyCDs Oven.

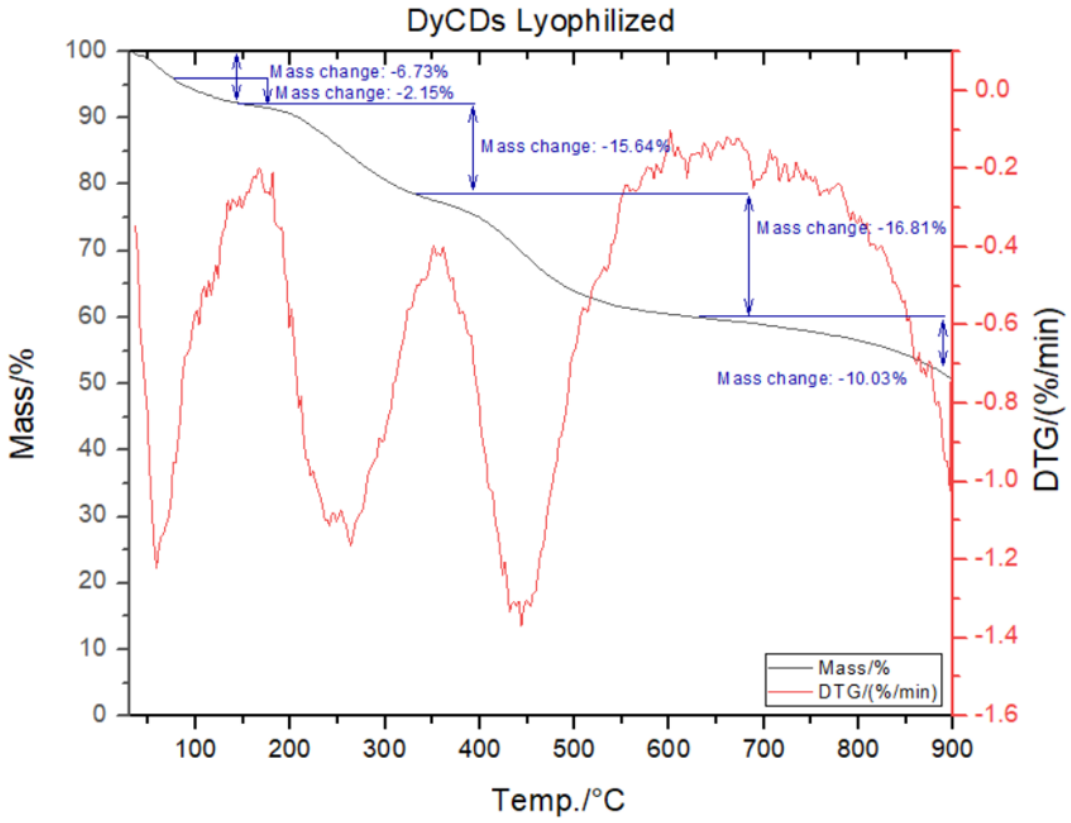


Fig. 4.16: TGA of DyCDs Lyophilized.

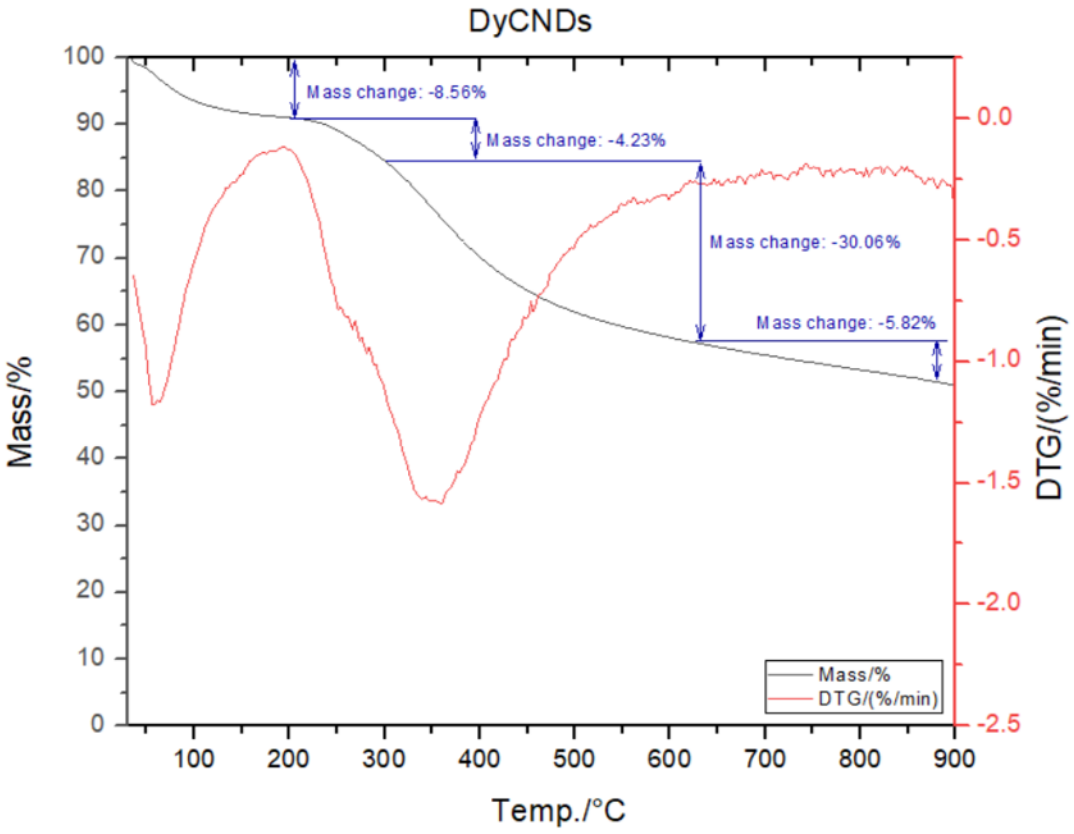


Fig. 4.17: TGA of DyCNDs.

## 4.2.7 Mass Spectrometry (MALDI-TOF)

Mass spectrometry has been used to quantify carbon dots and the presence of other compounds, such as side products or unreacted precursors. Through the analysis, it was assessed the molecular weight of the carbon dots (568.314 Da DyCDs oven, 568.319 Da DyCDs lyophilized 568.410 Da DyCNDs). The molecular weight of carbon dots was important to evaluate if the dialysis 500 Da cut-off membrane could work or not. In Fig. 4.18, the most relevant fractions have been reported. It is shown that the molecular weight of the other two fractions is close to 500 Da, meaning that the efficacy of the membrane is sufficient. We do not notice the presence of clusters, considering that the fractions share similar values.

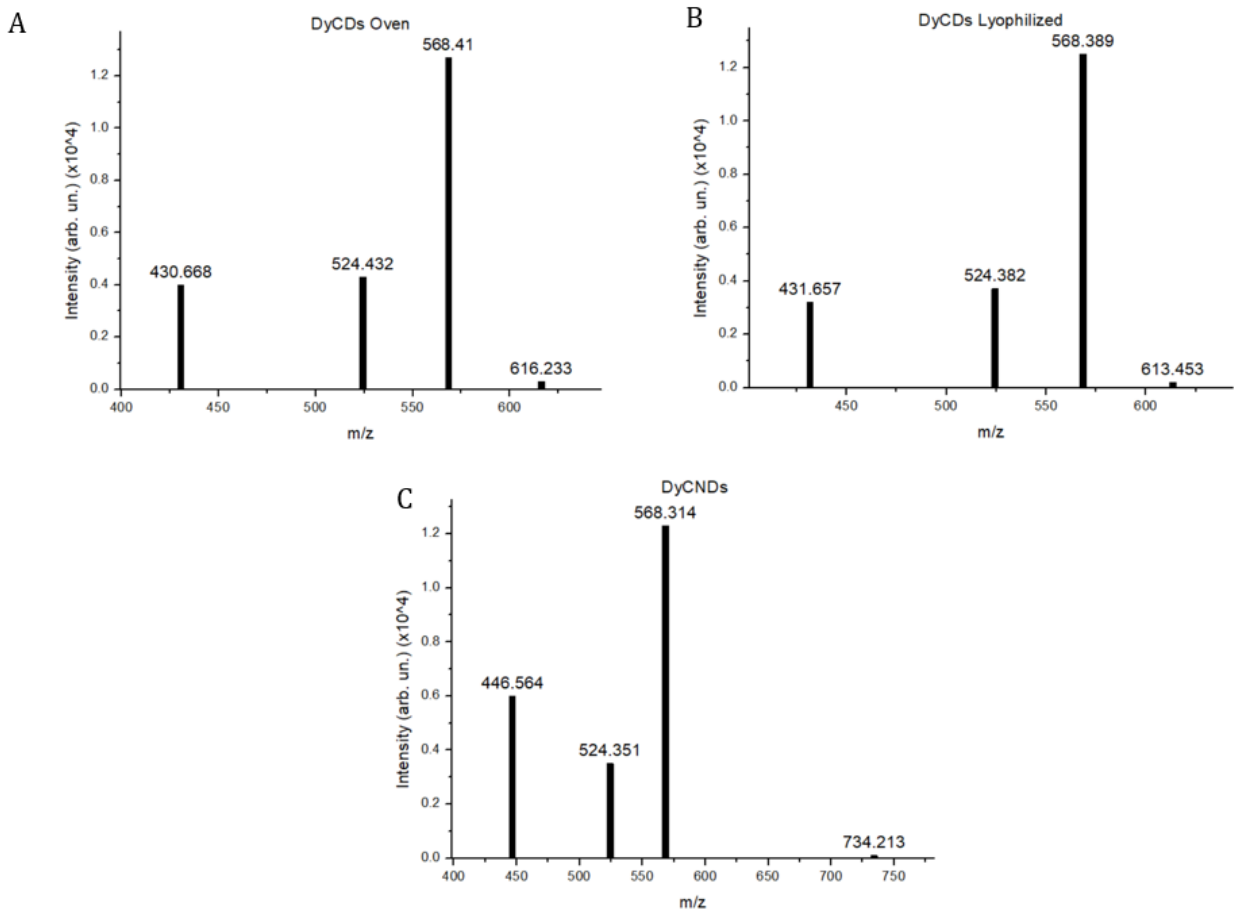


Fig. 4.18: The most relevant DyCDs and DyCNDs fractions of MALDI spectra have been reported.

## 4.2.8 Electronic Paramagnetic Resonance Spectroscopy

EPR is a spectroscopic technique for determining the structure, the dynamics and spatial distribution of paramagnetic species, i.e., species, containing at least an unpaired electron. Both EPR and NMR examine how magnetic dipoles interact with an applied magnetic field, as well as with the right wavelength of electromagnetic radiation. EPR is concerned with the splitting of electronic spin states, whereas NMR is concerned with the splitting of nuclear spin states under a magnetic field [60]. EPR was performed to evaluate the paramagnetic properties of the prepared C-dots and to extrapolate T1 and T2 relaxation times. Dysprosium's 4f orbitals are half-filled. Dysprosium ion (3+) presents five unpaired electrons, and it shows paramagnetic properties above 179°K.

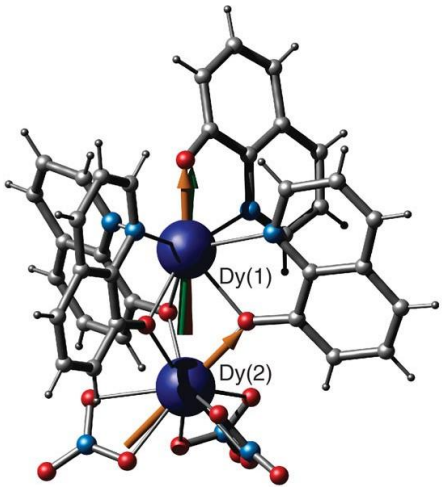


Fig. 4.19: Paramagnetic properties of $Dy^{3+}$ [62].

EPR was used to examine the ground-state properties of the prepared C-dots. The analysis was performed on Dy-CDs Oven, Dy-CDs lyophilized and DyCNDs. EPR spectra were collected at room temperature. For each sample, the analysis was conducted by varying the power: 0.1 mW, 0.2 mW, 0.5mW, 1Mw, 2mW, 5mW, 10mW. The peak was found in the field range 3400-3500 Gauss (0.34-0.35 Tesla).

From the plots, it was found a g value for each sample. The found g values are respectively 2.0025964 for Dy-CDs Oven, 2.0022379 for Dy-CDs Lyophilized and 2.0024786 for DyCNDs. These values suggest the presence of singly occupied orbitals [61].

EPR spectra of the three samples are shown in Fig. 4.20.

The reduction of the g value that can be seen in DyCNDs could be explained by the changes in half-filled orbitals of C-dots because of the differences in the synthesized nanoparticles.

As can be seen from Fig. 4.21, since the synthesized carbon dots do not show a saturation behaviour, T1 and T2 relaxation times could not be extrapolated.

| **SAMPLE** | **G VALUE** |
|---|---|
| DY-CDS OVEN | 2.0025964 |
| DY-CDS LYOPHILIZED | 2.0022379 |
| DY-CNDS | 2.0024786 |

Table 4.2: C-dots' g values.

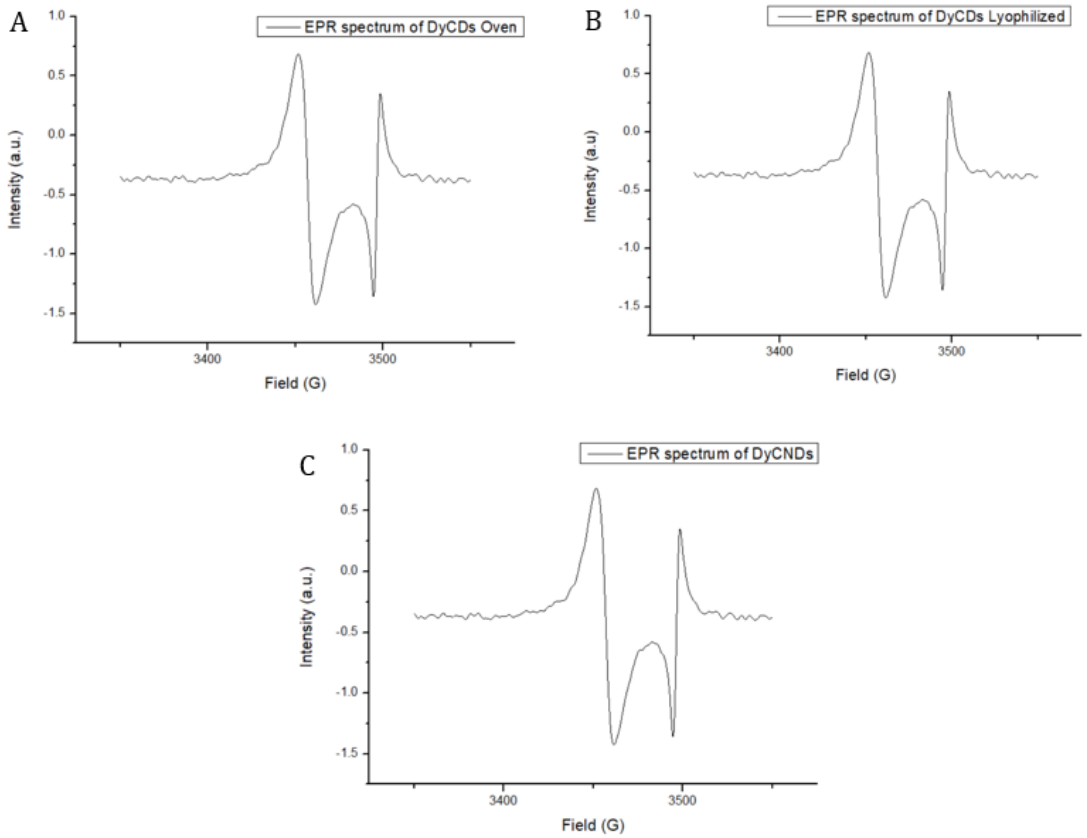


Fig. 4.20: EPR spectra of the prepared C-dots.

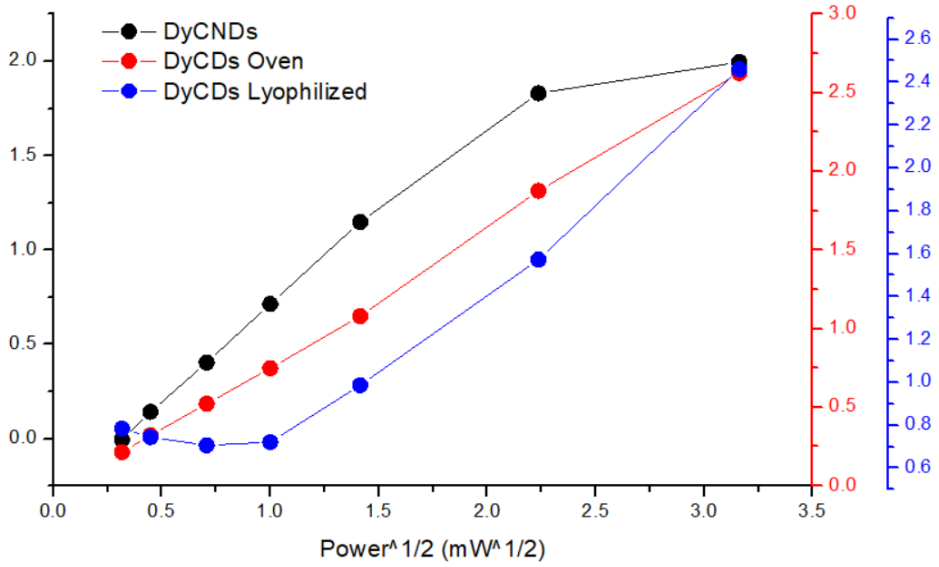


Fig. 4.21: EPR saturation curves.

### 4.2.9 Cellular tests: viability

In experimental research, it is necessary to compare the results of two or more measurements with each other. Such comparison can be made by appropriate statistical tests. To this end, ANOVA was adopted as the selected statistical method.

For the purposes of the project, it was critical to evaluate how target cells interacted with the carbon dots. In literature [63], there are a few comparison studies concerning viability tests on carbon dots. The majority of toxicity and viability tests have been conducted on epithelial cells and fibroblasts [63]. In this work, four cell types have been investigated: SK-N-AS and SK-N-BE2C (Human neuroblastoma cells), MSC (Mesenchymal Stem Cells) and VSMC (Vascular Smooth Muscle Cells).

Figures 4.22, 4.23 and 4.24 show the cell survival rate after 24 hours of treatment with carbon dots at concentrations of 10 μg/ml, 100 μg/ml, 250 μg/ml. For each cell type, three classes of carbon dots were tested: oven-dried Dy-CDs (Dy-CDs Oven), Dy-CDs lyophilized, Dy-CNDs.

At concentrations up to 10 μg/ml, MSC, SK-N-AS and SK-N-BE2C are almost fully viable. VSMC show lower viability percentages especially when treated with lyophilized Dy-CDs and Dy-CNDs. No significant changes are reported when increasing the concentration up to 100 μg/ml. On the contrary, it is evident that from 250 μg/ml, cell viability decreases significantly. Overall, VSMC show lower viability than mesenchymal stem cells (MSC).

ANOVA comparison tests were used to assess if the differences that could be noticed when increasing the concentration, changing the cell line, or treating cells with a different type of carbon dots were due to chance or could be associated with a particular behavior. The statistical analysis proved that it is possible to extrapolate some trends from the viability data. Values were considered significant at $p < 0.05$.

In the following part, these trends will be further explained and analyzed.

As expected, it is evident a decrease in cell viability when the concentration is increased. For SK-N-BE2C and MSC the trend is more evident. When cells are treated with CNDs viability goes from 86.2% (10 μg/ml) to 46.7% (250 μg/ml) for SK-N-BE2C and from 94.34% (10 μg/ml) to 71.6% (250 μg/ml) for MSC.

Another interesting point concerns the type of C-dots that were used to treat the cells. One of the goals of the viability tests was to assess which type of C-dots could work better and was less toxic. DyCDs Oven show overall higher viability rates compared to lyophilized Dy-CDs and CNDs. Concerning SK-N-AS and SK-N-BE2C, it is remarkable that when the cells are treated with DyCNDs the viability decreases with higher concentrations. However, for lyophilized DyCDs this trend is not valid. For CDs Oven, it is possible to notice a step decrease from 100 μg/ml to 250 μg/ml.

MSC show a similar behaviour. In this case, higher concentrations of lyophilized CDs cause a decrease in the viability, but this hypothesis cannot be generalized because it is not valid for all CD types and cell lines. Regarding VSMC, for oven-dried and lyophilized CDs we could think of a gradual decrease in viability from 10 μg/ml to 250 μg/ml, that is not present for CNDs.

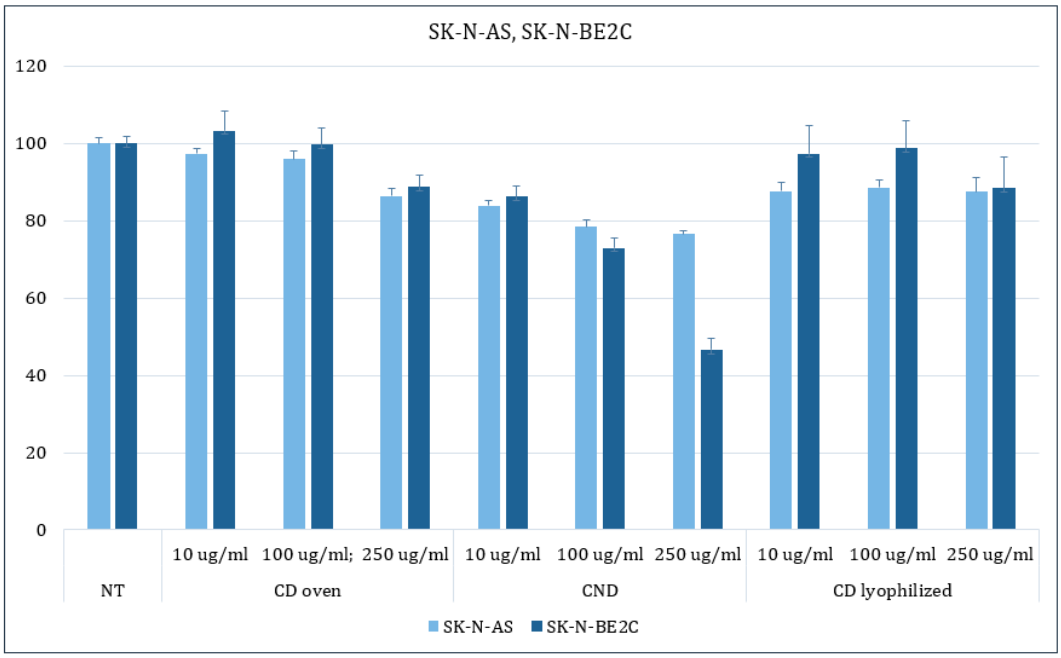


Fig. 4.22: Fig. 4.23: Viability of SK-N-AS and SK-N-BE2C treated with different concentration of DyCDs Oven, DyCDs Lyophilized and DyCNDs.

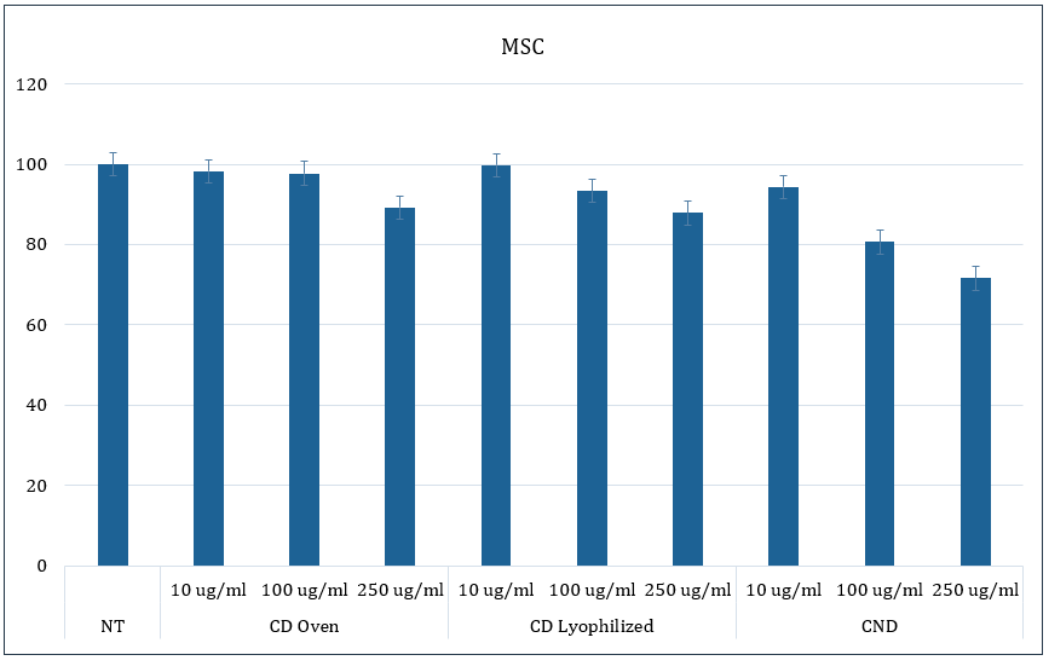


Fig. 4.23: Viability of MSC treated with different concentration of DyCDs Oven, DyCDs Lyophilized and DyCNDs.

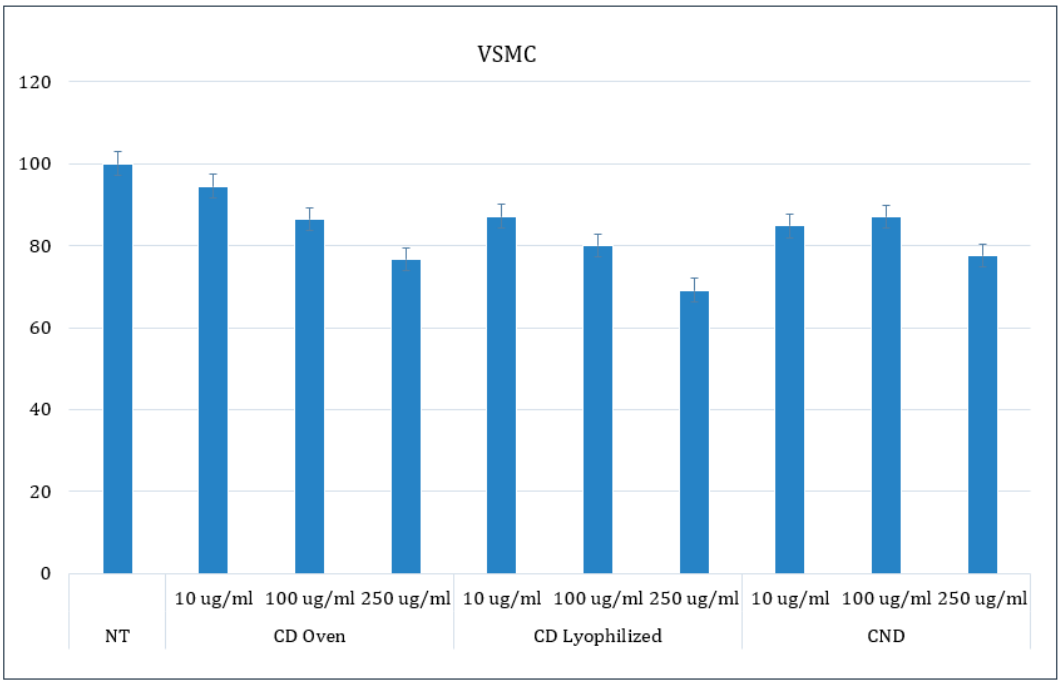


Fig. 4.24: Viability of VSMC treated with different concentration of DyCDs Oven, DyCDs Lyophilized and DyCNDs.

## 4.2.10 Cellular imaging

C-dots may be an excellent option for bioimaging in living biological organisms due to their above-mentioned photoluminescence characteristics, low toxicity, and good water solubility. The excitation-dependent emission is a crucial feature, allowing the imaging of cells at different wavelengths.

First, through cellular imaging it was pointed out the presence of crystalline composites Fig. 4.25. It was hypothesized that these impurities could increase the toxicity of the prepared C-dots and could interfere with the mechanism of cellular internalization. For this reason, it was implemented a NaOH filtration to remove these residues. In filtrated C-dots (Fig. 4.25) there were still some nano-dimensional crystalline parts, but the size of the latter ones should not largely affect the cell-particles interaction.

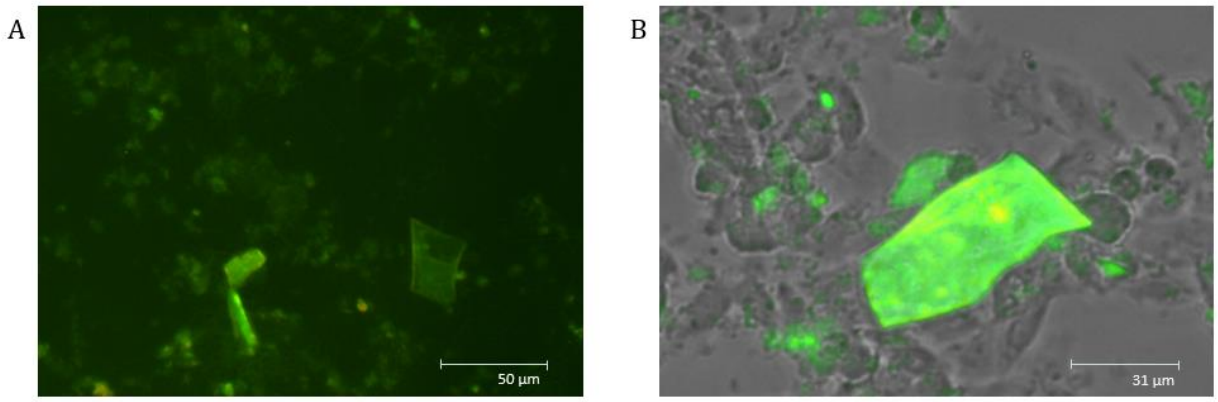


Fig. 4.25: Crystalline composites seen through cellular imaging before NaOH filtration of DyCNDs.

It was observed that the dots entered the cell cytoplasm with no negative effects on the viability or shape of the cell. The cells were visualized in both green and red fluorescence (Fig. 4.26, Fig. 4.27). The C-dots interacted more efficiently with the cytoplasm than with the nuclei, as seen by the lower fluorescence intensity in cell nuclei compared to the one in the cytoplasm. Due to the C-dots' size, it was hypothesized that they might enter cells through diffusion across the cell membrane. Moreover, C-dots entering the SK-AS-BE2C cells proved that it was possible to proceed in the desired direction and begin the next step of conjugation.

Through the previous characterization, it was determined that C-dots had functional groups similar to glutamine, such as carboxylic groups[64]. Thus, using the ASCT2 transporter (amino acid transporter localized in the plasma membrane), CNDs could penetrate the cancer cells as if they were glutamine. In fact, it is largely known that cancer cells consume more glutamine to support growth and proliferation during malignant transformation. Indeed, recent promising anti-cancer therapies aim to target the metabolism of glutamine.

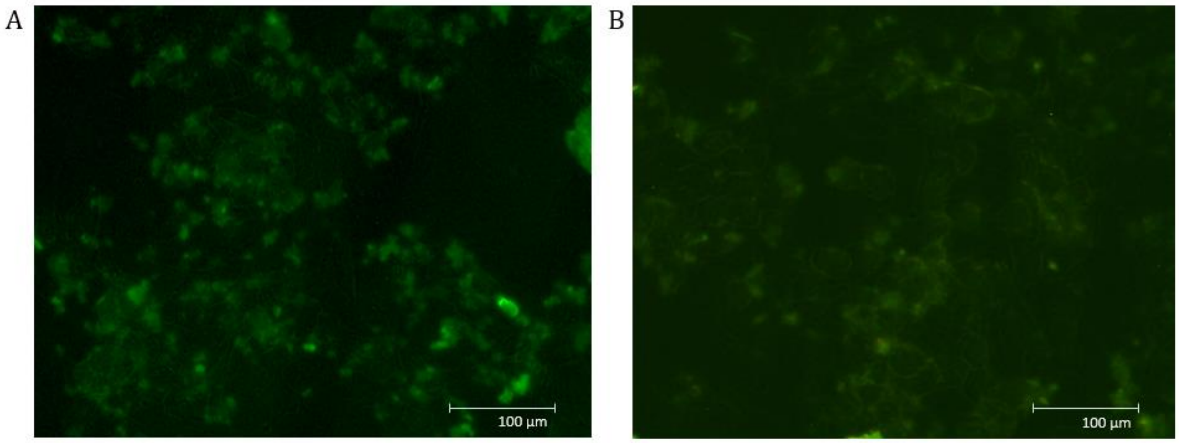


Fig. 4.26: Cellular imaging, green fluorescence of SK-N-BE2C treated with filtrated DyCNDs.

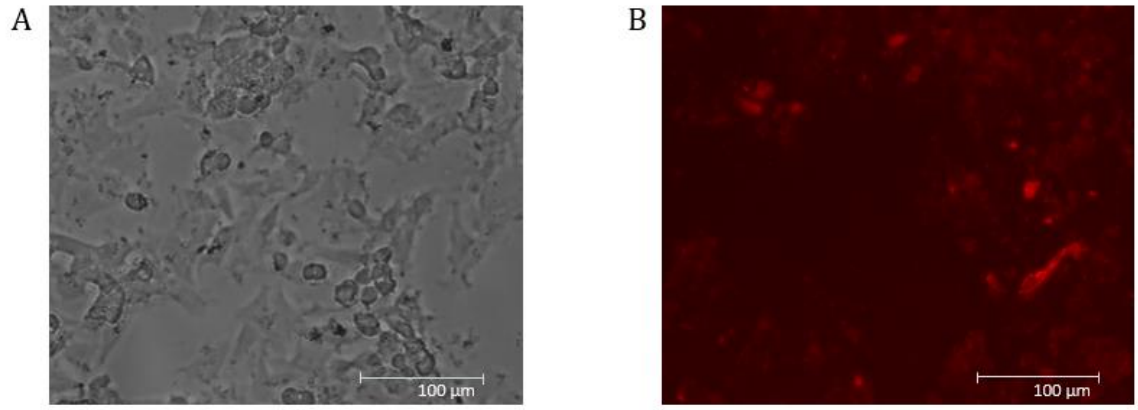


Fig. 4.27: Bright field and red fluorescence of SK-N-BE2C treated with filtrated DyCNDs.

## 4.3 Doxorubicin-conjugated C-Dots

Due to larger size of the nanoparticles after conjugation, the majority of dual nano drug delivery systems fail to penetrate malignant brain tumors [65]. In fact, nanoparticles can reach a dimension of 100 nm, while the synthesized C-dots have a diameter of around 3-4 nm. In this work, we aimed to create a double-conjugated system containing dysprosium and doxorubicin. As previously seen, C-dots are doped with dysprosium for its paramagnetic properties while doxorubicin is selected as anti-cancer drug.

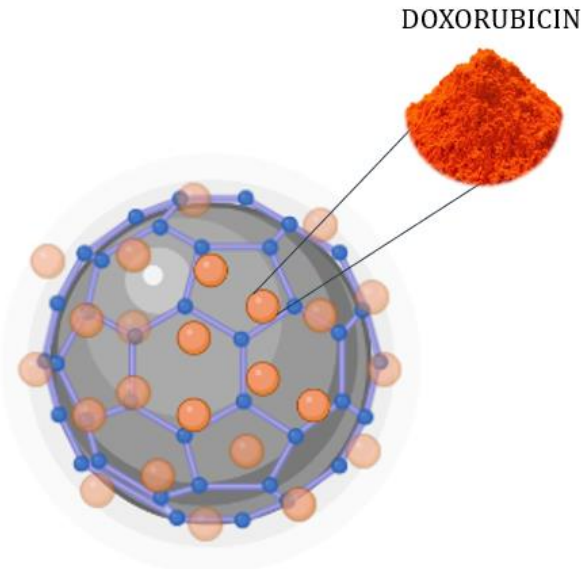


Fig. 4.28: Dy-CNDs conjugated with doxorubicin [66].

An EDC/NHS coupling was applied to conjugate the CNDs and doxorubicin.

Doxorubicin is an antibiotic generated from the bacterium Streptomyces peucetius, largely used as a chemotherapeutic agent. Doxorubicin is frequently used as a medication to treat solid tumors in both adult and pediatric patients. Cancers of the breast, ovary, bladder, and thyroid can all be treated with doxorubicin. Doxorubicin's main method of action is its capacity to intercalate among DNA base pairs, breaking DNA strands and inhibiting the creation of both DNA and RNA. Plus, Topoisomerase II is inhibited by doxorubicin, which results in DNA damage and the activation of apoptosis [67].

During the conjugation process, doxorubicin was carefully managed, considering its sensitivity to light and heat.

In the following part, FT-IR and fluorescence spectroscopy will be discussed to show the successful conjugation of doxorubicin.

### 4.3.1 Fluorescence Spectroscopy

The fluorescence properties of doxorubicin are used to evaluate the drug's distribution after administration and the drug's behaviour with the DNA [68]. Doxorubicin water solution shows a reddish/orange, fluorescent color. From literature [68,69], it is known that doxorubicin's fluorescence emission is around 600 nm with an excitation wavelength of 480 nm. In Fig. 4.29 the spectra of doxorubicin, DyCNDs and DyCNDs conjugated with doxorubicin (DyCNDs-DOXO) are reported. The spectrum of the DyCNDs-DOXO can be seen as a convolution of the spectra of the two components, showing a first peak around 520 nm and a second one around 600 nm.

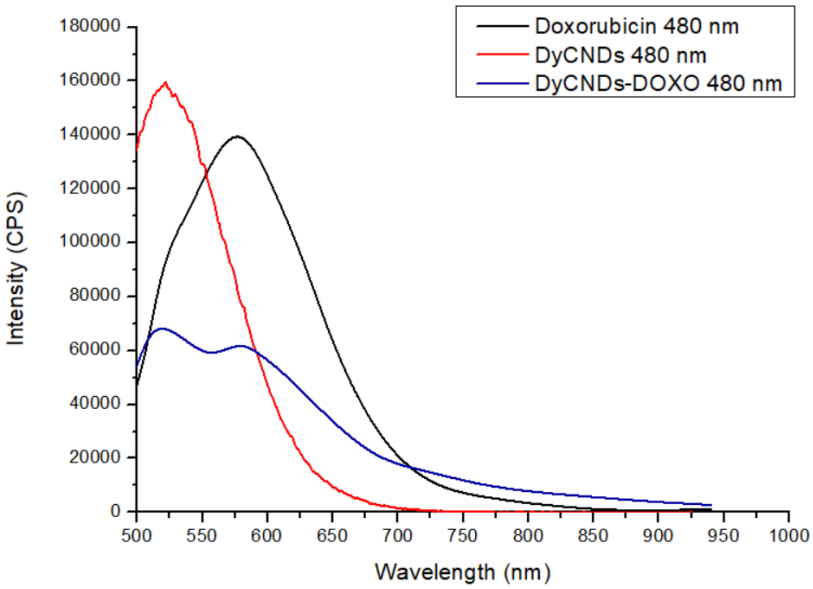


Fig. 4.29: Fluorescence spectra of doxorubicin, DyCNDs and DyCNDs-DOXO at an excitation wavelength of 480nm [66].

## 4.3.2 FT-IR Spectroscopy

Fig. 4.30 and Fig. 4.31 show the FT-IR spectra of doxorubicin, DyCNDs and DyCNDs-DOXO. It is remarkable that DyCNDs-DOXO show similar peaks to both DyCNDs and doxorubicin. They share with DyCNDs the majority of bands, such as the O-H stretching at 3435 $cm^{-1}$, the C-N stretching at 1773 $cm^{-1}$, the C=C ring stretching at 1614 $cm^{-1}$. On the other hand, the C-H stretching at 2935 $cm^{-1}$, the C=O stretching at 1729 $cm^{-1}$, the C-O-C stretching at 1068 $cm^{-1}$ and the C=C bending at 692 $cm^{-1}$ are probably due to the presence of doxorubicin.

FT-IR gives some insight into the surface chemistry of the conjugated C-dots. This type of information would be interesting for future conjugations and cell interactions. In fact, a possible further step would be the conjugation of DyCNDs-DOXO with a ligand, such as the aptamer AS1411, for a better tumour targeting. AS1411 recognizes and binds to nucleolin, which is overexpressed on the surface of certain cancer cells [70].

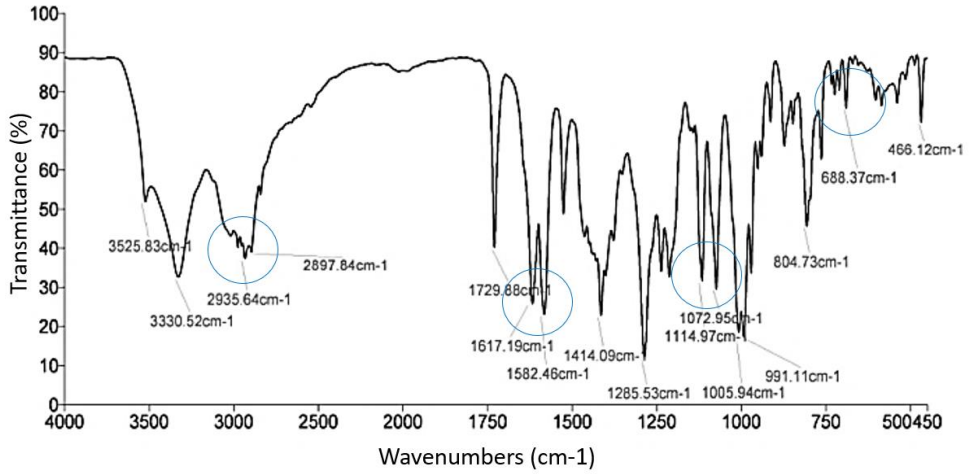


Fig. 4.30: IR spectrum of doxorubicin [71].

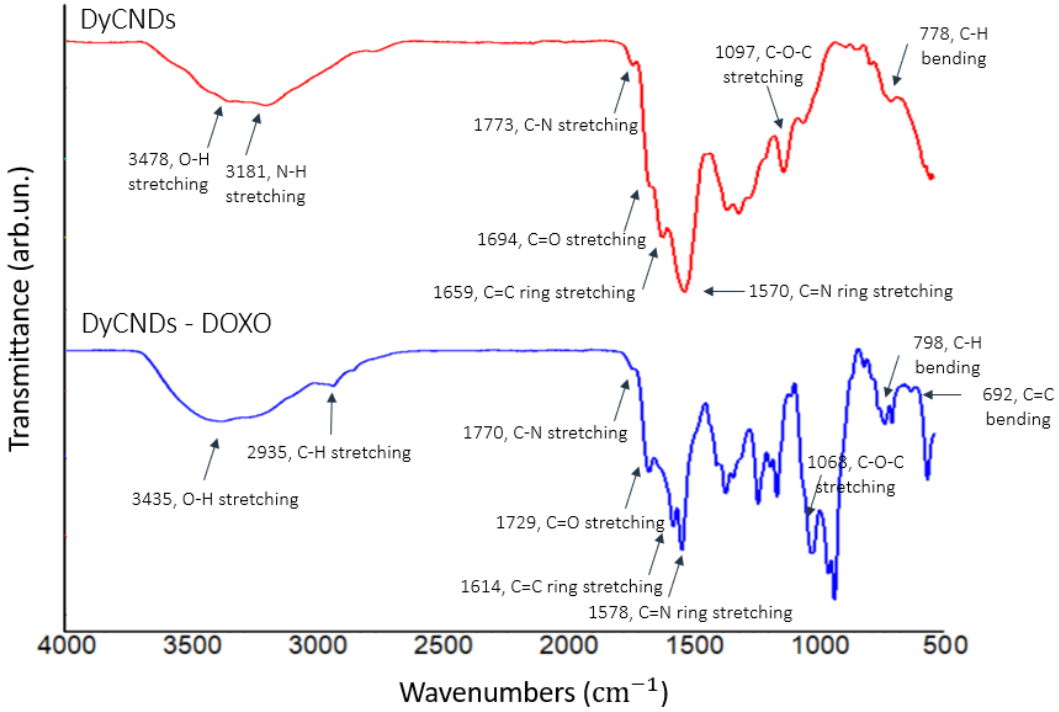


Fig. 4.31: IR spectra of DyCNDs and DyCNDs-DOXO.

The conjugated-complex was originally thought for neuroblastoma treatment, a nerve pediatric cancer [77]. Pediatric tumours are difficult to treat especially for their fast expansion and modification [78]. Therefore, a theranostic tool would be useful to follow constantly the treatment and evaluate its efficacy. Personalised medicine has a great relevance for paediatric patients [79,80].

Here, it is showed that doxorubicin can be easily attached to the C-dot. However, more tests are needed to assess both relaxometric and cell interaction properties after conjugation.

Fig. 4.32: Design of a C-dots-based theranostic tool for neuroblastoma [81].

# CHAPTER 5
# CONCLUSIONS

In conclusion, a few synthesis of C-dots were conducted and their characteristics were compared to determine which compound would be the greatest fit for biomedical purposes.

The purpose of the project was to synthesize dysprosium-doped carbon dots that could be used as MRI contrast agents taking advantage of dysprosium's paramagnetic properties. Finally, the C-dots were conjugated with doxorubicin for cancer treatment.

The synthesized C-dots are promising because of their outstanding fluorescence, paramagnetic, and surface properties which made it possible to design a theranostic tool. C-dots can be used for bioimaging applications because of their high quantum yield, strong stability, and low cytotoxicity.

The work was divided into synthesis, characterization, conjugation, and tests. The preparation of the precursors for the thermal syntheses was the first step in the experimental process. A one-pot synthesis method was adopted to form the dysprosium-doped carbon dots. Two classes of C-dots were synthesized: carbon dots with dysprosium chloride hexahydrate and citric acid as precursors, and carbon nitride dots, adding urea to the precursors set. An optimization process was performed to evaluate how to prepare fluorescent, non-toxic C-dots that could be suitable as MRI contrast agents and functionalized with a chemotherapeutic drug. The precursors were stirred overnight, then heated in a domestic microwave (700W for 7 minutes) where the C-dots were carbonized. After, they were purified through centrifugation, NaOH filtration, and dialyzed for three days in a 500 Da cut-off dialysis membrane to remove side products and unreacted particles. Finally, they were dried in a laboratory oven or lyophilized. Both oven-dried and lyophilized C-dots were selected to be further analyzed.

The characterization step was performed in parallel with the synthesis to grant better results. The optical properties of the C-dots were assessed through UV-Vis, fluorescence, and FT-IR spectroscopy. UV-Vis spectroscopy helped to assess the formation of the C-dots. Fluorescence spectra showed intense excitation-dependent emission, especially of the DyCNDs due to the presence of urea in the precursors set. Then, AFM was used to evaluate the dimension and shape of the particles proving that the prepared C-dots are spherical with a diameter of about 3-4 nm. A Thermogravimetric Analysis was conducted to study the composition of the C-dots. Through MALDI-TOF, it was assessed that the molecular mass of the particles was around 568 Da for all the samples. This analysis proved that the most relevant fractions had a similar molecular weight and that no clusters were present. Zeta potential was conducted to evaluate the colloidal stability of the C-dots solution. Nanostructured contrast agents are usually dispersed in water solutions; thus, the potential of the particles must not threaten the stability of the solution and its injection. From the analysis, it was discovered that both DyCDs and DyCNDs are almost neutral. Therefore, further tests are needed to evaluate the particle coalescence when the C-dots are solubilized.

The purpose of using Electron Paramagnetic Spectroscopy was to extrapolate from the data the C-dots' T1 and T2 relaxation times. Unfortunately, the curves were not saturated, hence it was not possible to calculate T1 and T2. Instead, it was obtained a g value of the particles which was respectively 1.963 for DyCDs Oven, 1.958 for Dy-CDs Lyophilized and 1.932 for Dy-CNDs.

Subsequently, cellular tests were conducted to assess the interaction of the C-dots with the cells. Four cell lines were treated with the samples: SK-N-AS and SK-N-BE2C (neuroblastoma cell lines), MSC and VSMC. Overall, the C-dots did not show high toxicity and the survival rate was higher than 80% for all the cell lines treated with a concentration of 10 μg/ml. However, the viability slightly decreased with higher concentrations (100 μg/ml, 250 μg/ml). Through ANOVA tests, it was assessed a decrease in viability due to higher concentrations. Plus, it was observed that the viability rates changed according to the C-dots sample used to treat the cells. For lyophilized DyCDs, no significant trends were observed, while for DyCNDs it was evident that the higher the concentration the lower the survival rate.

Cellular imaging was conducted on SK-N-BE2C treated with DyCNDs, showing a good interaction of the C-dots with the cells. It was hypothesized the diffusion of the C-dots through the cell membrane. In fact, C-dots carboxyl surface groups are similar to glutamine, which is overexpressed in tumor tissues [64]. Thus, using the ASCT2 transporter (amino acid transporter localized in the plasma membrane), CNDs could penetrate cancer cells.

Doxorubicin was conjugated to DyCNDs using an EDC/NHS coupling method. DyCNDs were selected among the other C-dots for two main reasons: their fluorescence was more intense and, through titration it was assessed a strong presence of surface carboxylic groups which are fundamental for the conjugation and the formation of the carbodiimide bond.

Then, the conjugated complex was characterized through fluorescence and FT-IR Spectroscopy. Thanks to these techniques, it was stated the success of the conjugation and formation of the DyCNDs-DOXO complex. In this context, a further step would consist of functionalizing the complex with the aptamer A1411 to better target and penetrate tumor tissues.

More studies are needed to evaluate the efficacy of the conjugated complex as a theranostic tool. First, NMR would be necessary to extrapolate the T1 and T2 relaxation times. Plus, more cellular tests are required to better understand the particle-cell interaction, the drug release, and the fluorescence intensity. Moreover, if the nanomaterial could successfully penetrate the tumor, this might be a labeling tool for cancer diagnosis and therapy, follow-up, and even image-guided surgery.

# ACKNOWLEDGEMENTS

First and foremost, I would like to express my deepest gratitude to my primary supervisor, Prof. Alberto Tagliaferro, for giving me the opportunity to work on this project providing valuable guidance and feedback.

I would like to express my deepest appreciation to Prof. Roger Leblanc for hosting me in his research group. I wish to acknowledge the help provided by the Department of Chemistry of the University of Miami.

I wish to extend my special thanks to Dr. Mattia Bartoli for his invaluable supervising and for guiding me throughout this project with patience, dedication, and constant support.

Words cannot express my gratitude to my family for their trust, strength, and unconditional love. To my Mum, Grazia, and my Dad, Renato. I could not have undertaken this journey without you. Thank you for always being my guiding light.

I would also like to thank my brother, Emanuele, my grandparents, Amalia, Maria Luisa, Bruno, Mario, and my beloved aunt, Silvia.

I feel extremely blessed for all the precious friends I had by my side during these years.

To my childhood best friend, Lucia, who has always challenged me to become a better person.

To Federica and Elisabetta, who supported me, understood me, and had my back since day one.

To Francesca, Annalisa, Chiara, and Martina, I will never forget all the obstacles we faced together and the wonderful moments we shared.

To Rachele, Carlotta, and all my friends not mentioned here, thank you for making me laugh like no one else. I am grateful for having you in my life.

To all the people who have been by my side, you are always in my heart.

# REFERENCES


1) J.O.S.H. Cleary, A.R. Guimarães, Magnetic Resonance Imaging, Editor(s): Linda M. McManus, Richard N. Mitchell, Pathobiology of Human Disease, Academic Press, 2014, Pages 3987-4004, ISBN 9780123864574, https://doi.org/10.1016/B978-0-12-386456-7.07609-7.
2) Rachel W. Chan, Justin Y.C. Lau, Wilfred W. Lam, Angus Z. Lau, Magnetic Resonance Imaging, Editor(s): Roger Narayan, Encyclopedia of Biomedical Engineering, Elsevier, 2019, Pages 574-587, ISBN 9780128051443, https://doi.org/10.1016/B978-0-12-801238-3.99945-8.
3) https://www.researchgate.net/publication/442077478/figure/fig1/AS:904126695227496@1592572010748/Magnetic-resonance-imaging-scans-of-the-patient-at-different-ages-A-Images-at-25.png Accessed 12/10/2022
4) Geethanath, S., & Vaughan, J. T. (2019). Accessible magnetic resonance imaging: A review. Journal of Magnetic Resonance Imaging, 49(7), e65–e77. https://doi.org/10.1002/jmri.26638
5) Grover, V. P. B., Tognarelli, J. M., Crossey, M. M. E., Cox, I. J., Taylor-Robinson, S. D., & McPhail, M. J. W. (2015). Magnetic Resonance Imaging: Principles and Techniques: Lessons for Clinicians. Journal of Clinical and Experimental Hepatology, 5(3), 246–255. https://doi.org/10.1016/j.jceh.2015.08.001
6) Gossuin, Y., Hocq, A., Gillis, P., & Quoc Lam, V. (2010). Physics of magnetic resonance imaging: From spin to pixel. Journal of Physics D: Applied Physics, 43(21). https://doi.org/10.1088/0022-3727/43/21/213001
7) Jenkins, F. A., & Segrè, E. (1939). The Quadratic Zeeman Effect. *Phys. Rev.*, *55*(1), 52–58. https://doi.org/10.1103/PhysRev.55.52
8) https://www.khanacademy.org/test-prep/mcat/physical-processes/proton-nuclear-magnetic-resonance/a/magnetic-resonance-imaging-mri Accessed: 10/10/2022
9) Jordan, D. (2020). State of the art in magnetic resonance imaging. Physics Today, 73(2), 34–40. https://doi.org/10.1063/PT.3.4408
10) K.J. Ooms, K. Genuis, K.W. Feindel, 3.326 - Imaging and Diagnosis of Biological Markers, Editor(s): Paul Ducheyne, Comprehensive Biomaterials,Elsevier,2011,Pages 427-446,ISBN 9780080552941, https://doi.org/10.1016/B978-0-08-055294-1.00113-6.
11) https://taninnit.com/wp-content/uploads/2019/09/taninnit.comknowledgedifference-mri-tesla.jpg Accessed: 12/10/2022
12) Yan, G. P., Robinson, L., & Hogg, P. (2007). Magnetic resonance imaging contrast agents: Overview and perspectives. Radiography, 13(SUPPLL. 1). https://doi.org/10.1016/j.radi.2006.07.005
13) Robillard, M., & Pharmaceuticals, T. (2014). Technical Note PR-TN 2005 / 00933 Targeted Agents for Imaging and Therapy. June.

14) Wahsner, J., Gale, E. M., Rodríguez-Rodríguez, A., & Caravan, P. (2019). Chemistry of MRI contrast agents: Current challenges and new frontiers. Chemical Reviews, 119(2), 957–1057. https://doi.org/10.1021/acs.chemrev.8b00363

15) https://upload.wikimedia.org/wikipedia/commons/thumb/8/85/Bluthirnschranke_nach_Infarkt_nativ_und_KM.png/220px-Bluthirnschranke_nach_Infarkt_nativ_und_KM.png Accessed: 10/10/2022

16) Fang, J., Islam, W., & Maeda, H. (2020). Exploiting the dynamics of the EPR effect and strategies to improve the therapeutic effects of nanomedicines by using EPR effect enhancers. *Advanced Drug Delivery Reviews*, *157*(2020), 142–160. https://doi.org/10.1016/j.addr.2020.06.005

17) Park, J., Choi, Y., Chang, H., Um, W., Ryu, J. H., & Chan, I. (2019). *Theranostics Alliance with EPR Effect : Combined Strategies to Improve the EPR Effect in the Tumor Microenvironment*. *9*(26). https://doi.org/10.7150/thno.3719

18) https://www.researchgate.net/publication/321242519/figure/fig3/AS:568113893527553@1512460315795/Accumulation-of-nanoparticles-in-tumor-tissues-via-the-EPR-effect.png

19) Pierre, V. C., Allen, M. J., & Caravan, P. (2014). Contrast agents for MRI: 30+ years and where are we going? Topical issue on metal-based MRI contrast agents. Guest editor: Valérie C. Pierre. Journal of Biological Inorganic Chemistry, 19(2), 127–131. https://doi.org/10.1007/s00775-013-1074-5

20) Hendrick, R. E., & Mark Haacke, E. (1993). Basic physics of MR contrast agents and maximization of image contrast. Journal of Magnetic Resonance Imaging, 3(1), 137–148. https://doi.org/10.1002/jmri.1880030126

21) Kostevšek, N. (2020). A Review on the Optimal Design of Magnetic Nanoparticle-Based T2 MRI Contrast Agents. *Magnetochemistry*, *6*(1). https://doi.org/10.3390/magnetochemistry6010011

22) https://encrypted-tbn1.gstatic.com/images?q=tbn:ANd9GcS37oHZojj-Am2w62antV-wu-FAtZopEDqGjAwF2wIS8JLyOK_l Accessed: 12/10

23) Xiao, Y. D., Paudel, R., Liu, J., Ma, C., Zhang, Z. S., & Zhou, S. K. (2016). MRI contrast agents: Classification and application (Review). *International Journal of Molecular Medicine*, *38*(5), 1319–1326. https://doi.org/10.3892/ijmm.2016.2744

24) Wahsner, J., Gale, E. M., Rodríguez-Rodríguez, A., & Caravan, P. (2019). Chemistry of MRI contrast agents: Current challenges and new frontiers. *Chemical Reviews*, *119*(2), 957–1057. https://doi.org/10.1021/acs.chemrev.8b00363

25) Babes, L., Denizot, B., Tanguy, G., Le Jeune JJ, & Jallet, P. (1999). Synthesis of Iron Oxide Nanoparticles Used as MRI Contrast Agents: A Parametric Study. *Journal of colloid and interface science*, *212*(2), 474–482. https://doi.org/10.1006/jcis.1998.6053

26) Caspani, S., Magalhães, R., Araújo, J. P., & Sousa, C. T. (2020). Magnetic nanomaterials as contrast agents for MRI. *Materials*, *13*(11). https://doi.org/10.3390/ma13112586

27) Pierre, V. C., Allen, M. J., & Caravan, P. (2014). Contrast agents for MRI: 30+ years and where are we going? Topical issue on metal-based MRI contrast agents. Guest editor: Valérie C. Pierre. *Journal of Biological Inorganic Chemistry*, *19*(2), 127–131. https://doi.org/10.1007/s00775-013-1074-5

28) Hao, D., Ai, T., Goerner, F., Hu, X., Runge, V. M., & Tweedle, M. (2012). MRI contrast agents: Basic chemistry and safety. *Journal of Magnetic Resonance Imaging*, *36*(5), 1060–1071. https://doi.org/10.1002/jmri.23725

29) Shellock, F. G., & Kanal, E. (1999). Safety of magnetic resonance imaging contrast agents. *Journal of Magnetic Resonance Imaging*, *10*(3), 477–484. https://doi.org/10.1002/(SICI)1522-2586(199909)10:3<477::AID-JMRI33>3.0.CO;2-E

30) Peng, E., Wang, F., & Xue, J. M. (2015). Nanostructured magnetic nanocomposites as MRI contrast agents. *Journal of Materials Chemistry B*, *3*(11), 2241–2276. https://doi.org/10.1039/c4tb02023e

31) https://www.researchgate.net/publication/269182214/figure/fig2/AS:294990375866370@1447342594517/Different-types-of-nanoparticles-commonly-used-for-biomedical-applications-and-which.png Accessed: 12/10/2022

32) F. Pacheco-Torgal, Said Jalali, Nanotechnology: Advantages and drawbacks in the field of construction and building materials, Construction and Building Materials,Volume 25, Issue 2, 2011, Pages 582-590,ISSN 0950-0618, https://doi.org/10.1016/j.conbuildmat.2010.07.009. (https://www.sciencedirect.com/science/article/pii/S0950061810003764)

33) Marasini, R., Thanh Nguyen, T. D., & Aryal, S. (2020). Integration of gadolinium in nanostructure for contrast enhanced-magnetic resonance imaging. *Wiley Interdisciplinary Reviews: Nanomedicine and Nanobiotechnology*, *12*(1), 1–17. https://doi.org/10.1002/wnan.1580

34) Niculescu, V. C. (2020). Mesoporous Silica Nanoparticles for Bio-Applications. *Frontiers Shen, Z., Wu, A., & Chen, X. (2016). Iron Oxide Nanoparticle Based Contrast Agents for Magnetic Resonance Imaging. Molecular Pharmaceutics, 14(5),* 1352–1364. https://doi.org/10.1021/acs.molpharmaceut.6b00839

35) Yaqoob, Asim Ali & Ahmad, Hilal & Parveen, Tabassum & Ahmad, Akil & M., Oves & Ismail, Iqbal & Qari, Huda & Umar, Khalid & Ibrahim, Mohamad. (2020). Recent Advances in Metal Decorated Nanomaterials and Their Various Biological Applications: A Review. Frontiers in Chemistry. 8. 10.3389/fchem.2020.00341.

36) Svenson, S. (2013). *Theranostics : Are We There Yet ?*

37) Jeelani, S., Reddy, R. C., Maheswaran, T., Asokan, G. S., Dany, A., & Anand, B. (2014). Theranostics: A treasured tailor for tomorrow. *Journal of pharmacy & bioallied sciences*, *6*(Suppl 1), S6–S8. https://doi.org/10.4103/0975-7406.137249

38) https://ars.els-cdn.com/content/image/1-s2.0-S0169409X1000164X-fx1.jpg Accessed: 10/10/2022

39) Tuerhong, M., XU, Y., & YIN, X. B. (2017). Review on Carbon Dots and Their Applications. *Chinese Journal of Analytical Chemistry*, *45*(1), 139–150. https://doi.org/10.1016/S1872-2040(16)60990-8

40) Campuzano, S., Yáñez-Sedeño, P., & Pingarrón, J. M. (2019). Carbon dots and graphene quantum dots in electrochemical biosensing. *Nanomaterials*, *9*(4), 1–18. https://doi.org/10.3390/nano9040634

41) Xia, C., Zhu, S., Feng, T., Yang, M., & Yang, B. (2019). Evolution and Synthesis of Carbon Dots: From Carbon Dots to Carbonized Polymer Dots. *Advanced Science*, *6*(23). https://doi.org/10.1002/advs.201901316

42) https://www.renishaw.it/media/img/en/50e033cc197a416db28909dc584e38a1.jpg Accessed: 10/10/2022

43) Mansuriya, B. D., & Altintas, Z. (2021). Carbon dots: Classification, properties, synthesis, characterization, and applications in health care-an updated review (2018–2021). *Nanomaterials*, *11*(10). https://doi.org/10.3390/nano11102525

44) Zhou, Y., Sharma, S. K., Peng, Z., & Leblanc, R. M. (2017). Polymers in carbon dots: A review. *Polymers*, *9*(2), 67. https://doi.org/10.3390/polym9020067

45) Liu, M. L., Chen, B. Bin, Li, C. M., & Huang, C. Z. (2019). Carbon dots: Synthesis, formation mechanism, fluorescence origin and sensing applications. *Green Chemistry*, *21*(3), 449–471. https://doi.org/10.1039/c8gc02736f

46) Abid, N., Khan, A. M., Shujait, S., Chaudhary, K., Ikram, M., Imran, M., Haider, J., Khan, M., Khan, Q., & Maqbool, M. (2022). Synthesis of nanomaterials using various top-down and bottom-up approaches, influencing factors, advantages, and disadvantages: A review. *Advances in Colloid and Interface Science*, *300*(December 2021), 102597. https://doi.org/10.1016/j.cis.2021.102597

47) Wang, X., Feng, Y., Dong, P., & Huang, J. (2019). A Mini Review on Carbon Quantum Dots: Preparation, Properties, and Electrocatalytic Application. *Frontiers in Chemistry*, *7*(October), 1–9. https://doi.org/10.3389/fchem.2019.00671

48) Koutsogiannis, P., Thomou, E., Stamatis, H., Gournis, D., & Rudolf, P. (2020). Advances in fluorescent carbon dots for biomedical applications. Advances in Physics: X, 5(1). https://doi.org/10.1080/23746149.2020.1758592

49) Zhu, S., Song, Y., Zhao, X. *et al.* The photoluminescence mechanism in carbon dots (graphene quantum dots, carbon nanodots, and polymer dots): current state and future perspective. *Nano Res.* **8**, 355–381 (2015). https://doi.org/10.1007/s12274-014-0644-3

50) https://www.edinst.com/wp-content/uploads/2019/05/carbon-dots-1.png Accessed: 10/10/2022

51) Liyanage, P. Y., Graham, R. M., Pandey, R. R., Chusuei, C. C., Mintz, K. J., Zhou, Y., Harper, J. K., Wu, W., Wikramanayake, A. H., Vanni, S., & Leblanc, R. M. (2019). Carbon Nitride Dots: A Selective Bioimaging Nanomaterial. *Bioconjugate Chemistry*, *30*(1), 111–123. https://doi.org/10.1021/acs.bioconjchem.8b00784

52) Hinterberger, V., Damm, C., Haines, P., Guldi, D. M., & Peukert, W. (2019). Purification and structural elucidation of carbon dots by column chromatography. *Nanoscale*, *11*(17), 8464–8474. https://doi.org/10.1039/c9nr01029g

53) Bart, J., Tiggelaar, R., Yang, M., Schlautmann, S., Zuilhof, H., & Gardeniers, H. (2009). Room-temperature intermediate layer bonding for microfluidic devices. *Lab on a Chip*, *9*(24), 3481–3488. https://doi.org/10.1039/b914270c

54) Fischer, M.J.E. (2010). Amine Coupling Through EDC/NHS: A Practical Approach. In: Mol, N., Fischer, M. (eds) Surface Plasmon Resonance. Methods in Molecular Biology, vol 627. Humana Press. https://doi.org/10.1007/978-1-60761-670-2_3

55) https://www.researchgate.net/profile/Han-Gardeniers/publication/40731516/figure/fig1/AS:277324571398149@1443130738982/EDC-NHS-chemistry-EDC-reacts-with-a-carboxylic-acid-group-on-FEP-sheet-indicated-by.png Accessed: 10/10/2022

56) Villanueva, E., Navarro, P., Rovira-Rigau, M., Sibilio, A., Méndez, R., & Fillat, C. (2017). Translational reprogramming in tumour cells can generate oncoselectivity in viral therapies. *Nature Communications*, *8*. https://doi.org/10.1038/ncomms14833

57) Mintz, K. J., Bartoli, M., Rovere, M., Zhou, Y., Hettiarachchi, S. D., Paudyal, S., Chen, J., Domena, J. B., Liyanage, P. Y., Sampson, R., Khadka, D., Pandey, R. R., Huang, S., Chusuei, C. C., Tagliaferro, A., & Leblanc, R. M. (2021). A deep investigation into the structure of carbon dots. *Carbon*, *173*, 433–447. https://doi.org/10.1016/j.carbon.2020.11.017

58) De, B., & Karak, N. (2013). A green and facile approach for the synthesis of water soluble fluorescent carbon dots from banana juice. *RSC Advances*, *3*(22), 8286–8290. https://doi.org/10.1039/c3ra00088e

59) Fiuza, T., Gomide, G., Campos, A. F. C., Messina, F., & Depeyrot, J. (2019). On the Colloidal Stability of Nitrogen-Rich Carbon Nanodots Aqueous Dispersions. *C — Journal of Carbon Research*, *5*(4), 74. https://doi.org/10.3390/c5040074

60) Yan, F., Sun, Z., Zhang, H., Sun, X., Jiang, Y., & Bai, Z. (2019). The fluorescence mechanism of carbon dots, and methods for tuning their emission color: a review. *Microchimica Acta*, *186*(8). https://doi.org/10.1007/s00604-019-3688-y

61) Wang, K., Geng, C., Wang, F., Zhao, Y., & Ru, Z. (2021). Urea-doped carbon dots as fluorescent switches for the selective detection of iodide ions and their mechanistic study. *RSC Advances*, *11*(44), 27645–27652. https://doi.org/10.1039/d1ra04558j

62) Carbonaro, Corpino, Salis, Mocci, Thakkar, Olla, & Ricci. (2019). On the Emission Properties of Carbon Dots: Reviewing Data and Discussing Models. *C — Journal of Carbon Research*, *5*(4), 60. https://doi.org/10.3390/c5040060

63) Latief, U., ul Islam, S., Khan, Z. M. S. H., & Khan, M. S. (2021). A facile green synthesis of functionalized carbon quantum dots as fluorescent probes for a highly selective and sensitive detection of Fe3+ ions. *Spectrochimica Acta - Part A: Molecular and Biomolecular Spectroscopy*, *262*, 120132. https://doi.org/10.1016/j.saa.2021.120132

64) Pudza, M. Y., Abidin, Z. Z., Rashid, S. A., Yasin, F. M., Noor, A. S. M., & Issa, M. A. (2020). Eco-friendly sustainable fluorescent carbon dots for the adsorption of heavy metal ions in aqueous environment. *Nanomaterials*, *10*(2). https://doi.org/10.3390/nano10020315

65) Roessler, M. M., & Salvadori, E. (2018). Principles and applications of EPR spectroscopy in the chemical sciences. *Chemical Society Reviews*, *47*(8), 2534–2553. https://doi.org/10.1039/c6cs00565a

66) Lin, Z., Xue, W., Chen, H., & Lin, J. M. (2012). Classical oxidant induced chemiluminescence of fluorescent carbon dots. *Chemical Communications*, *48*(7), 1051–1053. https://doi.org/10.1039/c1cc15290d

67) https://media.springernature.com/lw685/springer-static/image/art%3A10.1038%2Fncomms6243/MediaObjects/41467_2014_Article_BFncomms6243_Fig1_HTML.jpg?as=webp Accessed: 10/10/2022

68) Navarro-Ruiz, M. C., Cayuela, A., Soriano, M. L., Guzmán-Ruiz, R., Malagón, M. M., & Valcárcel, M. (2020). A systematic comparative study of the toxicity of semiconductor and graphitic carbon-based quantum dots using in vitro cell models. *Applied Sciences (Switzerland)*, *10*(24), 1–16. https://doi.org/10.3390/app10248845

69) Nguyen, T. L., & Durán, R. V. (2018). Glutamine metabolism in cancer therapy. *Cancer Drug Resistance*, *1*(3), 126–138. https://doi.org/10.20517/cdr.2018.08

70) Lungu, I. I., Nistorescu, S., Badea, M. A., Petre, A. M., Udrea, A. M., Banici, A. M., Fleacă, C., Andronescu, E., Dinischiotu, A., Dumitrache, F., Staicu, A., & Balaş, M. (2020). Doxorubicin-conjugated iron oxide nanoparticles synthesized by laser pyrolysis: In vitro study on human breast cancer cells. *Polymers*, *12*(12), 1–18. https://doi.org/10.3390/polym12122799

71) https://haihangchem.com/wp-content/uploads/2020/06/doxorubicin-hydrochloride-cas-25316-40-9.jpg Accessed: 10/10/2022

72) Johnson-Arbor, K., & Dubey, R. (2022). *Doxorubicin*. StatPearls Publishing, Treasure Island (FL). http://europepmc.org/books/NBK459232

73) Karukstis, K. K., Thompson, E. H. Z., Whiles, J. A., & Rosenfeld, R. J. (1998). Deciphering the fluorescence signature of daunomycin and doxorubicin. *Biophysical Chemistry*, *73*(3), 249–263. https://doi.org/10.1016/S0301-4622(98)00150-1

74) Behera, S. K., Mohanty, M. E., & Mohapatra, M. (2021). A Fluorescence Study of the Interaction of Anticancer Drug Molecule Doxorubicin Hydrochloride in Pluronic P123 and F127 Micelles. *Journal of Fluorescence*, *31*(1), 17–27. https://doi.org/10.1007/s10895-020-02630-y

75) Tong, X., Ga, L., Ai, J., & Wang, Y. (2022). Progress in cancer drug delivery based on AS1411 oriented nanomaterials. *Journal of Nanobiotechnology*, *20*(1), 1–36. https://doi.org/10.1186/s12951-022-01240-z

76) https://media.springernature.com/lw685/springerstatic/image/art%3A10.1186%2s13065-021-00752-3/MediaObjects/13065_2021_752_Fig2_HTML.png Accessed: 10/10/2022

77) Nour-Eldin, N. E. A., Abdelmonem, O., Tawfik, A. M., Naguib, N. N. N., Klingebiel, T., Rolle, U., Schwabe, D., Harth, M., Eltoukhy, M. M., & Vogl, T. J. (2012). Pediatric primary and metastatic neuroblastoma: MRI findings. Pictorial review. *Magnetic Resonance Imaging*, *30*(7), 893–906. https://doi.org/10.1016/j.mri.2012.02.028

78) Pui, C. H., Gajjar, A. J., Kane, J. R., Qaddoumi, I. A., & Pappo, A. S. (2011). Challenging issues in pediatric oncology. *Nature Reviews Clinical Oncology*, *8*(9), 540–549. https://doi.org/10.1038/nrclinonc.2011.95

79) Van Arendonk, K. J., & Chung, D. H. (2019). Neuroblastoma: Tumor biology and its implications for staging and treatment. *Children*, *6*(1). https://doi.org/10.3390/children6010012

80) Scarpa, M., Ceci, A., Tomanin, R., Mincarone, P., & Begley, D. (2011). Personalised medicine in paediatrics: Individualising treatment in children with rare neurological diseases. *EPMA Journal*, *2*(2), 231–239. https://doi.org/10.1007/s13167-011-0081-2

81) https://assets.medpagetoday.net/media/images/96xxx/96035.jpg Accessed: 13/10/2022